Received: 3 April 2021 | Revised: 30 April 2021 | Accepted: 23 May 2021

DOI: 10.1111/cbdd.13901

RESEARCH ARTICLE

WILEY

Rational design of novel *N*-alkyl amine analogues of noscapine, their chemical synthesis and cellular activity as potent anticancer agents

Rajesh Kumar Meher[1] | **Pratyush Pragyandipta**[1] | **Ravi K. Pedapati**[2] | **Praveen K. R. Nagireddy**[2] | **Srinivas Kantevari**[2] | **Arnab K. Nayek**[1] | **Pradeep K. Naik**[1]

[1]Department of Biotechnology and Bioinformatics, Centre of Excellence in Natural Products and Therapeutics, Sambalpur University, Sambalpur, India

[2]Fluoro and Agrochemicals Division, CSIR-Indian Institute of Chemical Technology, Hyderabad, India

Correspondence
Pradeep K. Naik, Department of Biotechnology and Bioinformatics, Centre of Excellence in Natural Products and Therapeutics, Sambalpur University, Sambalpur, India.
Email: pknaik1973@suniv.ac.in

Funding information
Indian Council of Medical Research (ICMR), Govt. of India, Grant/Award Number: 5/13/13/2019/NCD-III

Abstract

The scaffold structure of noscapine (an antitussive plant alkaloid) was modified by inducting *N*-aryl methyl pharmacophore at C-9 position of the isoquinoline ring to rationally design and screened three novel 9-(*N*-arylmethylamino) noscapinoids, **15–17** with robust binding affinity with tubulin. The selected 9-(*N*-arylmethylamino) noscapinoids revealed improved predicted binding energy of −6.694 kcal/mol for **15**, −7.118 kcal/mol for **16** and −7.732 kcal/mol for **17**, respectively in comparison to the lead molecule (−5.135 kcal/mol). These novel derivatives were chemically synthesized and validated their anticancer activity based on cellular studies using two human breast adenocarcinoma, MCF-7 and MDA-MB-231, as well as with a panel of primary breast tumor cells. These derivatives inhibited cellular proliferation in all the cancer cells that ranged between 3.2 and 32.2 μM, which is 11.9 to 1.8 fold lower than that of noscapine. These novel derivatives effectively arrest the cell cycle in the G2/M phase followed by apoptosis and appearance of apoptotic cells. Thus, we conclude that 9-(*N*-arylmethyl amino) noscapinoids, **15–17** have a high probability to be a novel therapeutic agent for breast cancers.

KEYWORDS

anticancer agents, breast cancer, *N*-arylmethylamino-noscapinoids, noscapine, tubulin binding

1 | INTRODUCTION

Noscapine is an opium alkaloid. It is non-narcotic, non-sedative and does not produce elation or addiction (Martindale, 1977). In the clinic, it has been used as orally available, safe antitussive drug for over 40 years. The ability of noscapine to bind microtubule, suppressing its dynamic instability and thereby inhibiting cell proliferation as well as induction of apoptosis encouraged a number of investigators to examine its anticancer potential (Jordan & Wilson, 2004; Landen et al., 2002; Ye et al., 1998; Zhou, Gupta, et al., 2002). Toward increment of its anticancer potential, a number of synthetic derivatives were synthesized and evaluated (Landen et al., 2002, 2004; Ye et al., 1998; Zhou et al., 2003; Zhou, Panda, et al., 2002). Interestingly, unlike the classic microtubule-targeted agents, taxanes (that over polymerizes microtubules and bundles them) and vincas (that depolymerizes microtubules), noscapine and its derivatives do not significantly alter the polymer and monomer ratio of microtubules and were known as a "kindler" microtubule poison. From clinical prospective, noscapine is also very unique from many other microtubule-targeted agents in a sense that it is lacking of substantial cytotoxicity to normal cells. It is also demonstrated to have very little or no toxicity to healthy volunteers (Dahlström et al., 1982; Jensen et al., 1992; Karlsson

et al., 1990). It also possesses a very good pharmacokinetic and ADME profile (Aneja, Dhiman, et al., 2007; Aneja, Ghaleb, et al., 2007) and does not produce any major organ toxicities. In order to enhance its anticancer activity, several derivatives have been developed (called noscapinoids) without inducing considerable toxic effects to normal cells. The first-generation, halogenated (fluoro, chloro, bromo, and iodo-noscapine), nitro, amino and azido derivatives of noscapine analogs were developed by modification on the C-9 position of isoquinoline ring system of noscapine scaffold (Aneja et al., 2006a, 2006b; Naik, Chatterji, et al., 2011; Naik, Santoshi, et al., 2011; Santoshi et al., 2011). These derivatives were demonstrated to have more anticancer activity compared to noscapine. The second-generation derivatives were developed by alteration of the benzofuranone ring system of noscapine, giving rise to O-alkylated and acylated noscapinoids (Mishra et al., 2011). These derivatives revealed better activity compared to noscapine. The third-generation derivatives were generated through manipulation in the isoquinoline ring system by functionalization of "N" (Manchukonda et al., 2013). Many of these derivatives exhibited substantial antiproliferative activity with a panel of cancer cells of different tissue origin. We have also recently developed a panel of hybrid analogs of noscapine (biaryl-noscapinoids) by coupling the biaryl pharmacophore (Santoshi et al., 2015) with improved cytotoxic activity. All the noscapinoids bind at the interface of α- and β-tubulin, near to colchicine binding site thereby inhibits the progression of the cell cycle at G2/M phase and induced apoptotic cell death in cancer cells.

In this study, we approach to develop a panel of *N*-arylmethylamino derivatives of noscapine **15–17** by strategically modifying its scaffold structure. These derivatives were then chemically synthesized and demonstrated their anticancer activity based on a cellular study using two human breast cancer cell lines (MCF-7 and MDA-MB-231) and a panel of primary breast tumor cells. The novel derivatives, **15–17** were found to bind tubulin heterodimer with increased binding affinity, effectively inhibit cancer cell proliferation, arrest cancer cells in the G2/M phase and effectively induced apoptosis to cancer cells.

2 | MATERIALS AND METHODS

2.1 | Protein preparation

The PDB structure (PDB ID: 6Y6D, resolution 2.20 Å, Oliva et al., 2020) of tubulin heterodimer was used for the in silico study. Although the crystal structure was obtained at high resolution, the missing hydrogen atoms were added and the structure was prepared using the multistep procedure of protein preparation wizard (Schrodinger). The structure was refined by energy minimization using Macromodel (Schrodinger). OPLS 2005 force field was used with Polak-Ribiere Conjugate Gradient (PRCG) algorithm and energy gradient of 0.01 kcal/mol. The structure was further refined by performing an all-atom molecular dynamics (MD) simulation of 100 ns in explicit water using GROMACS 4.5.4 software (Berendsen et al., 1995) and the GROMOS96 force field as reported earlier (Santoshi & Naik, 2014). The top most five structures with the lowest minimum total energy from the MD trajectory were used to generate the average structure of the tubulin.

2.2 | Rational design of *N*-alkyl amine derivatives of noscapine

From the literature, it is evident that modification on the C-9 position of the isoquinoline ring system of noscapine scaffold with halogens (fluoro, chloro, bromo, and iodo-noscapine), nitro, amino, and azido groups exerted to have enhanced anticancer activity compared to the parent compound, noscapine. Among these derivatives, 9-amino-noscapine is the most prominent one. Later studies predicted that further functionalization of groups at the C-9 position of the isoquinoline ring system could be the

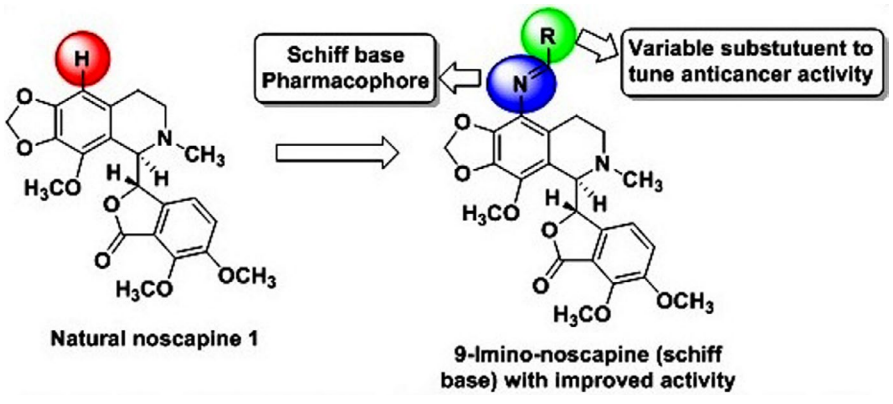

FIGURE 1 Strategic design of 9-(*N*-arylalkylamino) noscapinoids. The 9-amino group of noscapine was functionalize with alkyl or arylalkyl units to developed a library of 9-(*N*-arylalkylamino) noscapinoids

choice to tune the anticancer activity profile of noscapine. In this direction, we envisaged to functionalizing the 9-amino group of noscapine with alkyl or arylalkyl units to examine their anticancer potential. Initially, we have developed a library of *N*-arylalkylamino-noscapinoids by in silico combinatorial approach as depicted in Figure 1 followed by the screening of a panel of most potent compounds using a combination of both molecular docking and predictive binding free energy.

2.3 | Preparation of molecular structure of noscapinoids

Molecular structures of noscapinoids (Figure 2) that had been reported earlier (Aneja et al., 2006a; Manchukonda et al., 2013; Naik, Chatterji, et al., 2011; Naik, Santoshi, et al., 2011; Santoshi et al., 2011, 2015) and the newly designed *N*-arylalkylamino-noscapinoids (Figure 1) were built using ChemDraw and imported into Maestro (Schrödinger package). The molecular structures were energy minimized using Macromodel (Schrödinger package) and OPLS 2005 force field with PRCG algorithm (energy gradient of 0.001). The structures were further refined by geometric optimization using hybrid density functional theory with Becke's three-parameter exchange potential and the Lee-Yang-Parr correlation functional (B3LYP) with basis set 3-21G* using Jaguar (Schrödinger package). Further, the various conformations of each molecule were generated using Ligprep (Schrödinger package).

2.4 | Molecular docking of noscapinoids

The prepared molecular structures of noscapinoids were docked onto the αβ-tubulin heterodimer using Glide (Schrödinger package) as reported previously (Naik, Chatterji, et al., 2011; Naik, Santoshi, et al., 2011). Briefly, an inner grid box of size 12 Å × 12 Å × 12 Å was defined at the centroid of the binding site (Oliva et al., 2020) by selecting the co-complex ligand, amino-noscapine using Glide grid-receptor generation program. This box defines the search space in which the diameter midpoint of each docked ligand is required to be present. Further, an outer grid box was also defined with a size of ≤24 Å of the co-complexed ligand, amino-noscapine in the crystal structure. It defines the volume within which all ligand atoms of a valid pose must be located. All the noscapinoids were docked using Glide XP (extra precision) algorithm and evaluated their binding poses using Glide XP_{Score} function (Friesner et al., 2004; Halgren et al., 2004). The single best conformation for each ligand was used for further analysis.

2.5 | LIE-SGB model building

A robust predictive model was developed based on linear interaction energy model (LIE) with a surface generalized Born (SGB) continuum solvation model (Zhou et al., 2001) to determine the free energy of binding ($\Delta G_{bind,pred}$) of the newly designed *N*-arylalkylamino-noscapinoids with tubulin. A training data set of noscapinoids (Figure 2) with known experimental binding free energy, $\Delta G_{bind,expt}$ was used and mapped with various predicted energy parameters such as van der Waals (U_{vdw}), coulumbic (U_{coul}), reaction field (U_{rxn}) and cavity energy (U_{cav}) based on LIE model to develop the empirical prediction model. $\Delta G_{bind,expt}$ of noscapinoids with tubulin was determined from their respective dissociation constant (K_d) values using the relation:

$$\Delta G_{bind,expt} = RT \ln K_d$$

where R is gaseous constant (0.001986 kcal/mol) and T is the temperature (298 K). Liaison program (Schrödinger package) was used with the parameters set up as reported previously (Santoshi et al., 2015) to estimate the above

FIGURE 2 Molecular structures of previously reported noscapine derivatives that have experimentally proven to bind tubulin with known binding free energy (Table 1) and used as training test molecules for LIE-SGB building

energy parameters from the docked complexes of the noscapinoids based on Hybrid Monte Carlo simulation technique.

$$\Delta G_{\text{bind,pred}} = \alpha\left(\left\langle U^{b}_{\text{vdw}}\right\rangle - \left\langle U^{f}_{\text{vdw}}\right\rangle\right) + \beta\left(\left\langle U^{b}_{\text{coul}}\right\rangle - \left\langle U^{f}_{\text{coul}}\right\rangle\right) + \gamma\left(\left\langle U^{b}_{\text{rxn}}\right\rangle - \left\langle U^{f}_{\text{rxn}}\right\rangle\right) + \delta\left(\left\langle U^{b}_{\text{cav}}\right\rangle - \left\langle U^{f}_{\text{cav}}\right\rangle\right).$$

Here ⟨⟩ represents the ensemble average, *b* represents the bound form of the ligand, *f* represents the free form of the ligand, and α, β, γ and δ are the coefficients of the energy parameters. Finally based on the docking score and the predictive binding free energy, we have screened out the following three 9-(*N*-arylmethylamino) noscapinoids, **15–17** (Figure 3) having enhanced binding affinity with tubulin compared to noscapine for chemical synthesis and cellular evaluation to determine their anticancer potential.

2.6 | Molecular dynamics simulation

Molecular dynamics simulation of 100 ns was performed using GROMACS 2019.2 package (Abraham et al., 2015) for the docked complexes of tubulin and 9-(*N*-arylmethylamino) noscapinoids, **15–17**. The protein was processed by Gromacs with AMBER999SB force field (Hornak et al., 2006) to generate coordinates and topology files. The ligands parameters were defined using a general amber force field (GAFF) (Wang et al., 2004) implemented in the Antechamber program of Amber18. All atomic point charges were calculated using the AM1-BCC charge model (Jakalian et al., 2000, 2002). Topologies and internal coordinates of the complex were generated using the tleap program of Amber18 and ACPYPE software (Da Silva & Vranken, 2012). The molecular system was neutralized by adding counter-ions and solvation using the TIP3P water model in a truncated octahedron. The molecular system was relaxed and the bad contacts were removed by performing three rounds of minimization. Position restraints of 10 and 2 kcal/Å^2 were imposed on the molecular system for the first and the second round respectively, whereas no restraints were imposed in the third round. The molecular systems were equilibrated at 300 K and 1 atm for 500 ps. The equilibrated systems were then run for 100 ns each with a time step of 2 fm. Throughout simulations, the cut-off for non-bonded interaction was 10 Å, electrostatics were calculated using Particle Mesh Ewald (Essmann et al., 1995) and bonds were constrained using shake algorithm (Darden et al., 1993). Langevin thermostat was used to regulate the temperature of simulations. Co-ordinates were written every 20 ps to write 5,000 frames for each molecular system. CPPTAJ implemented in Ambertools was used to analyze trajectories for root mean square deviation analyses.

2.7 | Predictive binding affinity

Predicted binding affinity ($\Delta G_{\text{bind,pred}}$) of 9-(*N*-arylmethylamino) noscapinoids, **15–17** with tubulin was calculated using Molecular Mechanics Poisson-Boltzmann Surface Area (MM-PBSA). From the last 20 ns of MD trajectory, a total of 1,000 snapshots were extracted with a time step of 20 ps and the ensemble average of the $\Delta G_{\text{bind,pred}}$ was determined as reported earlier (Kollman et al., 2000).

$$\Delta G_{\text{bind,pred}} = \Delta G_{\text{complex}} - \left[\Delta G_{\text{Rec}} + \Delta G_{\text{lig}}\right].$$

$$G = E_{\text{gas}} + G_{\text{sol}} - TS.$$

$$E_{\text{gas}} = E_{\text{int}} + E_{\text{ele}} + E_{\text{vdw}}$$

$$G_{\text{sol}} = G_{\text{PB(GB)}} + G_{\text{sol - np}}$$

$$G_{\text{sol - np}} = \gamma \text{SAS}$$

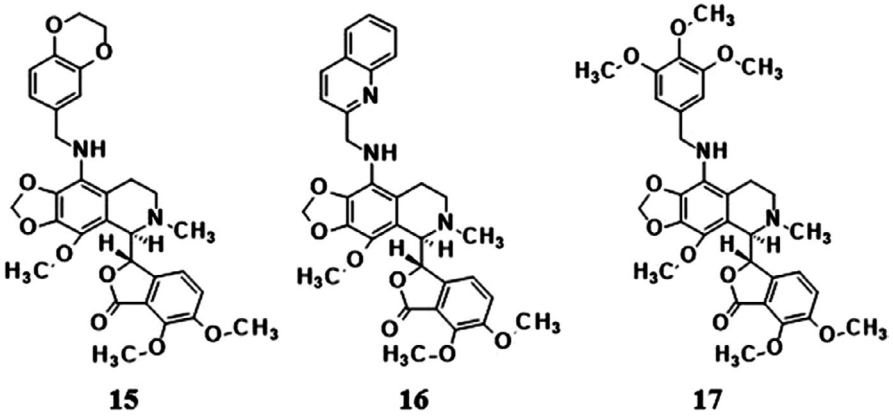

FIGURE 3 A panel of 9-(*N*-arylmethylamino) noscapinoids, **15–17** that are rationally designed and screened out to have higher binding affinity with tubulin for chemical synthesis and experimental evaluation

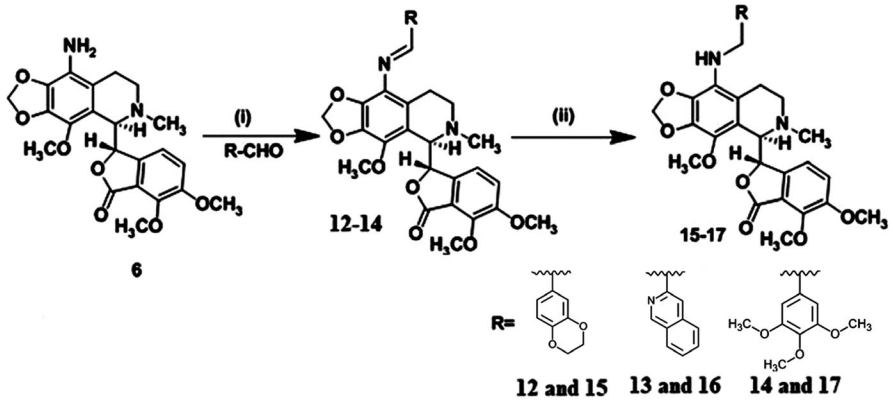

FIGURE 4 Synthesis of 9-(*N*-arylmethylamino) noscapinoids, **15–17**. Reaction conditions: (i) RCHO, EtOH, Reflux, 24 hr. (ii) $NaCNBH_3$, Methanol, RT, 4 hr. The 9-amino-noscapine was converted to 9-(arylimino) noscapinoids 12–14, which were then reduced to their respective 9-(*N*-arylmethylamino) noscapinoids

TABLE 1 Molecular docking results (Glide XP) as well as calculated energies using Liasion program (Schrodinger package) of noscapine and its derivatives: van der Waals energy (U_{vdw}), Columbic energy (U_{coul}), reaction energy (U_{rxn}) and cavity energy (U_{cav}) as well as predicted binding free energy ($\Delta G_{bind,pred}$) based on LIE-SGB prediction model and experimental binding free energy ($\Delta G_{bind,expt}$)

Ligand	Glide XP_{score} (kcal/mol)	$\langle U_{vdw} \rangle$ (kcal/mol)	$\langle U_{coul} \rangle$ (kcal/mol)	$\langle U_{rxn} \rangle$ (kcal/mol)	$\langle U_{cav} \rangle$ (kcal/mol)	Experimental ΔG_{bind} (kcal/mol)	Predicted ΔG_{bind} (kcal/mol)
1	−1.927	−45.14	−330.8	135.5	2.097	−5.246	−5.212
2	−2.038	−49.00	−210.2	116.0	3.283	−6.006	−6.178
3	−2.766	−42.50	−362.1	155.9	4.208	−5.827	−6.060
4	−2.940	−48.06	−355.8	168.7	2.548	−5.587	−5.899
5	−3.263	−47.69	−285.7	135.5	3.103	−6.360	−5.987
6	−4.492	−47.44	−77.3	118.2	3.954	−6.628	−6.668
7	−2.605	−33.39	−331.9	176.7	4.465	−5.551	−5.657
8	−2.287	−45.57	−277.9	112.3	3.285	−5.665	−5.706
9	−2.350	−33.47	−324.5	152.5	3.766	−5.783	−5.151
10	−3.679	−45.41	−471.2	152.8	3.669	−5.673	−5.790
11	−4.687	−42.69	−267.6	129.9	3.465	−5.518	−5.722
15	−4.175	−56.30	−268.8	122.9	3.766	Nd	−6.694
16	−4.208	−47.20	−422.3	193.8	5.486	Nd	−7.118
17	−3.941	−58.31	−266.2	137.7	5.473	Nd	−7.732

Note: The newly designed 9-(*N*-arylmethylamino) noscapinoids, **15–17** revealed improved $\Delta G_{bind,pred}$ compared to the lead molecule, noscapine.

$\langle U_{vdw} \rangle$, $\langle U_{coul} \rangle$, $\langle U_{rxn} \rangle$ and $\langle U_{cav} \rangle$ energy terms represents the ensemble average energy terms calculated as the difference between bound and free state of the ligands and its environment. Nd, not determined.

where G is Gibbs free energy, E_{gas} is the gas phase energy calculated as the sum of internal energy (E_{int}), energy generated as a result of the electrostatic interaction (E_{ele}) and the van der Waals interaction (E_{vdw}). G_{sol} is the solvation free energy calculated as the sum of polar (G_{PB}) and nonpolar contributions ($G_{sol\text{-}np}$). Polar interaction contribution (G_{PB}) was calculated as the summation of electrostatic contribution (E_{ele}) and polar solvation contribution (G_{PB}). The nonpolar solvation contribution ($G_{sol\text{-}np}$) is approximated as linearly dependent on the solvent accessible surface area (SAS) and γ is the surface tension constant that was set to 0.0072 kcal/mol $Å^{-2}$.

2.8 | Chemical synthesis of 9-(*N*-arylmethylamino)noscapinoids, 15–17

The natural α-noscapine was used as a starting material to produce 9-amino-noscapine via two reaction steps involving bromination of noscapine using aqueous HBr/Br_2-H_2O followed by amination using CuI, NaN_3 and L-Proline in DMSO as reported earlier (Manchukonda et al., 2014). A solution of 9-amino-noscapine **6** (1.0 mmol), in ethanol (15 ml), was refluxed with various substituted aromatic aldehydes (1.0 mmol), for 24 hr. After the compound was completely utilized in the reaction (judged by TLC), the

solvent was evaporated under a vacuum. The crude residue was extracted into dichloromethane (2 × 15 ml) and washed with brine solution. The organic layer was collected and passed through a Na_2SO_4 bed. The crude residue was chromatographed over a triethylamine silica bed, using petroleum ether/ethyl acetate (7:3) as eluents, to produce 9-(arylimino) noscapinoids **12–14** as solid products in very good yields. The synthesized **12–14** (1.0 mmol) were reduced to their respective 9-(*N*-arylmethylamino) noscapinoids, **15–17** by reacting them with sodium cyanoborohydride (1.2 mmol), in methanol (10 ml), for 4 hr at room temperature (Figure 4). Structural characterization of all the intermediates and final products were done using NMR (^{1}H and ^{13}C), IR spectroscopy and mass (HRMS) spectrometry techniques. The NMR (^{1}H and ^{13}C) and mass (HRMS) spectra of the 9-(*N*-arylmethylamino) noscapinoids, **15–17** were included in the supplementary material (S2–S10). All the synthesized compounds are HPLC purified using the C18 column (acetonitrile:water, 90:10) and were found to be >96.5% pure.

2.9 | Structural characterization of 9-(arylimino) noscapinoids, 12–14 and 9-(*N*-arylmethylamino) noscapinoids, 15–17

2.9.1 | (S)-6,7-dimethoxy-3-((R)-4-methoxy-6-methyl-9-((E)-(3,4,5-trimethoxybenzylidene) amino)-5,6,7,8-tetrahydro-[1,3]dioxolo[4,5-g] isoquinolin-5-yl)isobenzofuran-1(3H)-one (12)

Nature: White solid. M.P.: 124–126°C. IR (KBr): 3,493, 2,952, 2,899, 2,843, 2,794, 1,758, 1,628, 1,580, 1,499, 1,459, 1,390, 1,275, 1,122, 1,037, 1,006, 975, 846, 798, 727 cm^{-1}. ^{1}H NMR (400 MHz, $CDCl_3$): δ 8.73 (s, 1H, N=CH), 7.15 (s, 2H, Ar-H), 7.01 (d, J = 8.3 Hz, 1H, Ar-H), 6.35 (d, J = 8.3 Hz, 1H, Ar-H), 5.99 (dd, J = 1.3, 16.0 Hz, 2H, O-CH_2-O), 5.58 (d, J = 4.4 Hz, 1H, Ar-CH, (C3-phthalide)), 4.39 (d, J = 4.4 Hz, 1H, Ar-CH, (C5′-isoquinoline)), 4.10 (s, 3H, -OCH_3), 4.03 (s, 3H, -OCH_3), 3.94 (s, 6H, 2x -OCH_3), 3.91 (s, 3H, -OCH_3), 3.86 (s, 3H, -OCH_3), 3.01–2.91 (m, 1H, -C*H*H-*N*-CH_3 (C7′-isoquinoline)), 2.75–2.67 (m, 1H, -CH*H*-*N*-CH_3 (C7′-isoquinoline)), 2.55 (s, 3H, *N*-CH_3), 2.47–2.39 (m, 1H, Ar-C*H*H (C8′-isoquinoline)), 2.09–2.00 (m, 1H, Ar-CH*H* (C8′-isoquinoline)). ^{13}C NMR (100 MHz, $CDCl_3$): δ 168.1, 161.4, 153.4, 152.1, 147.6, 141.4, 140.8, 138.9, 138.6, 134.5, 132.3, 128.6, 125.8, 119.8, 118.4, 117.7, 105.3, 100.8, 81.7, 62.2, 60.9, 59.5, 56.7, 56.1, 54.8, 49.3, 45.8, 22.6. MS (ESI-MS) *m/z*: 607 [*M* + H] + HRMS (ESI): Calcd for $C_{32}H_{35}N_2O_{10}$ [*M* + H]+: 607.22862, found: 607.22803.

2.9.2 | (S)-6,7-dimethoxy-3-((R)-4-methoxy-6-methyl-9-((E)-(quinolin-3-ylmethylene)amino)-5,6,7,8-tetrahydro-[1,3]dioxolo[4,5-g]isoquinolin-5-yl)isobenzofuran-1(3H)-one (13)

Nature: White solid. M.P.: 120–122°C. IR (KBr): 3,446, 2,929, 2,794, 1,757, 1,626, 1,498, 1,443, 1,382, 1,268, 1,036, 1,007, 970, 763 cm^{-1}. ^{1}H NMR (400 MHz, $CDCl_3$): δ 9.22 (s, 1H, N=C*H*), 8.35 (d, J = 8.5 Hz, 1H, Ar-H), 8.23–8.15 (m, 2H, Ar-H), 7.86 (d, J = 7.9 Hz, 1H, Ar-H), 7.79–7.74 (m, 1H, Ar-H), 7.62–7.57 (m, 1H, Ar-H), 7.00 (d, J = 8.3 Hz, 1H, Ar-H), 6.31 (d, J = 8.3 Hz, 1H, Ar-H), 6.04 (d, J = 0.9, 17.7 Hz, 2H, O-C*H*2-O), 5.59 (d, J = 4.4 Hz, 1H, Ar-H, (C3-phthalide)), 4.42 (d, J = 4.4 Hz, 1H, Ar-H, (C5′-isoquinoline)), 4.10 (s, 3H), 4.07 (s, 3H), 3.85 (s, 3H), 3.16–3.06 (m, 1H, -C*H*H-N-CH_3 (C7′-isoquinoline)), 2.78–2.70 (m, 1H, -CH*H*-N-CH_3 (C7′-isoquinoline)), 2.57 (s, 3H, -N-C*H*$_3$), 2.49–2.40 (m, 1H, Ar-C*H*H (C8′-isoquinoline)), 2.14–2.03 (m, 1H, Ar-CH*H* (C8′-isoquinoline)). ^{13}C NMR (75 MHz, $CDCl_3$) δ 168.0, 161.8, 155.8, 152.1, 147.9, 147.6, 141.2, 139.77, 139.72, 136.3, 134.4, 130.1, 129.7, 129.5, 128.7, 127.6, 127.4, 124.5, 119.8, 118.2, 118.0, 117.7, 117.6, 101.1, 81.7, 62.2, 60.8, 59.4, 56.7, 49.4, 45.9, 22.9. MS (ESI-MS) *m/z*: 568 [*M* + H] + HRMS (ESI): Calcd for $C_{32}H_{30}N_3O_7$ [*M* + H]+: 568.20783, found: 568.20704.

2.9.3 | (S)-3-((R)-9-((E)-((2,3-dihydrobenzo[b][1,4]dioxin-6-yl)methylene)amino)-4-methoxy-6-methyl-5,6,7,8-tetrahydro-[1,3]dioxolo[4,5-g] isoquinolin-5-yl)-6,7-dimethoxyisobenzo furan-1(3H)-one (14)

Nature: White solid. M.P.: 155–157°C. IR (KBr): 3,423, 2,928, 2,796, 1,759, 1,629, 1,578, 1,430, 1,383, 1,294, 1,268, 1,068, 1,034, 1,007, 971, 885 cm^{-1}. ^{1}H NMR (400 MHz, $CDCl_3$): δ 8.71 (s, 1H, N=CH), 7.46 (d, J = 1.9 Hz, 1H, Ar-H), 7.36 (dd, J = 1.9, 8.4 Hz, 1H, Ar-H), 6.98 (d, J = 8.1 Hz, 1H, Ar-H), 6.93 (d, J = 8.3 Hz, 1H, Ar-H), 6.27 (d, J = 8.1 Hz, 1H, Ar-H), 5.98 (dd, J = 1.3, 15.5 Hz, 2H, O-C*H*$_2$-O), 5.58 (d, J = 4.2 Hz, 1H, Ar-CH, (C3-phthalide)), 4.39 (d, J = 4.2 Hz, 1H, Ar-CH, (C5′-isoquinoline)), 4.34–4.28 (m, 4H, O-C*H*$_2$-C*H*$_2$-O), 4.10 (s, 3H, -OCH_3), 4.03 (s, 3H, -OCH_3), 3.86 (s, 3H, -OCH_3), 2.99–2.90 (m, 1H, -C*H*H-*N*-CH_3 (C7′-isoquinoline)), 2.70–2.62 (m, 1H, -CH*H*-*N*-CH_3 (C7′-isoquinoline)), 2.54 (s, 3H, *N*-C*H*$_3$), 2.42–2.33 (m, 1H, Ar-C*H*H (C8′-isoquinoline)), 2.02–1.92 (m, 1H, Ar-CH*H* (C8′-isoquinoline)). ^{13}C NMR (100 MHz, $CDCl_3$): δ 168.1, 161.0, 152.1, 147.6, 146.4, 143.7, 141.3, 138.9, 138.4, 134.6, 130.8, 128.8, 125.9, 122.4, 119.9, 118.2, 117.7, 117.6, 117.4, 116.6, 100.8, 81.8, 64.5, 64.1, 62.2, 60.9, 59.5, 56.7, 49.5, 45.9, 22.8. MS (ESI-MS)

m/z: 575 [*M* + H] + HRMS (ESI): Calcd for $C_{31}H_{31}N_2O_9$ [*M* + H]+: 575.20241, found: 575.20129.

2.9.4 | (S)-6,7-dimethoxy-3-((R)-4-methoxy-6-methyl-9-((3,4,5-trimethoxybenzyl)amino)-5,6,7,8-tetrahydro-[1,3]dioxolo[4,5-g]isoquinolin-5-yl)isobenzofuran-1(3H)-one (15)

Nature: White solid. M.P.: 160–162°C. IR (KBr): 3,406, 2,943, 1,749, 1,591, 1,504, 1,460, 1,432, 1,318, 1,269, 1,123, 1,037, 1,009, 848 cm^{-1}. ^1H NMR (500 MHz, $CDCl_3$): δ 6.86 (d, *J* = 8.2 Hz, 1H, Ar-H), 6.56 (s, 2H, Ar-H), 6.02 (d, *J* = 8.2 Hz, 1H, Ar-H), 5.96 (dd, *J* = 1.2, 15.8 Hz, 2H, O-CH_2-O), 5.56 (d, *J* = 4.1 Hz, 1H, Ar-CH, (C3-phthalide)), 4.40 (d, *J* = 4.1 Hz, 1H, Ar-CH, (C5′-isoquinoline)), 4.29 (dd, *J* = 13.8, 51.5 Hz, 2H, *N*CH_2), 4.08 (s, 3H, -OCH_3), 3.94 (s, 3H, -OCH_3), 3.84 (s, 12H, 4x -OCH_3), 2.64–2.57 (m, 1H, -C*H*H-*N*-CH_3 (C7′-isoquinoline)), 2.52 (s, 3H, *N*-C*H*$_3$), 2.39–2.30 (m, 2H, -CH*H*-*N*-CH_3 (C7′-isoquinoline), Ar-C*H*H (C8′-isoquinoline)), 1.71–1.63 (m, 1H, Ar-CH*H* (C8′-isoquinoline)). ^{13}C NMR (100 MHz, $CDCl_3$): δ 168.0, 153.2, 152.1, 147.5, 140.9, 137.4, 137.1, 135.9, 135.3, 134.8, 124.2, 121.0, 119.9, 118.1, 117.6, 104.6, 100.6, 81.8, 62.2, 60.9, 60.7, 59.6, 56.7, 56.0, 51.4, 49.2, 45.8, 22.5. MS (ESI-MS) *m/z*: 609 [*M* + H] + HRMS (ESI): Calcd for $C_{32}H_{37}N_2O_9$ [*M* + H]+: 609.24427, found: 609.24513.

2.9.5 | (S)-6,7-dimethoxy-3-((R)-4-methoxy-6-methyl-9-((quinolin-2-ylmethyl)amino)-5,6,7,8-tetrahydro-[1,3]dioxolo[4,5-g]isoquinolin-5-yl) isobenzofuran-1(3H)-one (16)

Nature: White solid. M.P.: 96–98°C. IR (KBr): 3,380, 2,928, 1,757, 1,623, 1,498, 1,443, 1,268, 1,035, 967, 885, 821, 753, 474 cm^{-1}. ^1H NMR (400 MHz, $CDCl_3$): δ 8.35 (d, *J* = 8.5 Hz, 1H, Ar-H), 8.21 (d, *J* = 8.5 Hz, 1H, Ar-H), 8.17 (d, *J* = 8.5 Hz, 1H, Ar-H), 7.86 (d, *J* = 8.0 Hz, 1H, Ar-H), 7.78–7.73 (m, 1H, Ar-H), 7.62–7.57 (m, 1H, Ar-H), 7.03 (d, *J* = 8.3 Hz, 1H, Ar-H) 6.44 (d, *J* = 8.3 Hz, 1H, Ar-H), 6.03 (d, *J* = 19.0 Hz, 2H, O-CH_2-O), 5.93 (bs, 1H, -*NH*), 5.66 (d, *J* = 4.1 Hz, 1H, Ar-CH, (C3-phthalide)), 4.50 (d, *J* = 4.1 Hz, 1H, Ar-CH, (C5′-isoquinoline)), 4.11–4.06 (m, 4H, -*NC*H*H*, -OCH_3), 4.00 (s, 3H, -OCH_3), 3.87–3.83 (m, 4H, -*N*-CH*H*, -OCH_3), 3.16–3.08 (m, 1H, -C*H*H-*N*CH_3 (C7′-isoquinoline)), 2.91–2.81 (m, 1H, -CH*H*-N CH_3 (C7′-isoquinoline)), 2.63–2.52 (m, 4H, Ar-C*H*H (C8′-isoquinoline), *N*-CH_3), 2.28–2.16 (m, 1H, Ar-CH*H* (C8′-isoquinoline)). ^{13}C NMR (100 MHz, $CDCl_3$): δ 168.0, 161.9, 155.8, 152.2, 147.9, 147.6, 141.1, 140.0, 139.6, 137.8, 136.3, 134.4, 129.8, 129.6, 128.8, 127.7, 127.5, 124.5, 118.4, 118.0, 117.8, 116.7, 101.2, 81.5, 62.2, 60.9, 59.3, 56.7, 48.9, 47.6, 45.1, 22.4. MS (ESI-MS) *m/z*: 570 [*M* + H]+

2.9.6 | (S)-3-((R)-9-(((2,3-dihydrobenzo[b][1,4]dioxin-6-yl)methyl)amino)-4-methoxy-6-methyl-5,6,7,8-tetrahydro-[1,3]dioxolo[4,5-g]isoquinolin-5-yl)-6,7dimethoxyisobenzofuran-1(3H)-one (17)

Nature: White solid. M.P.: 73–75°C. IR (KBr): 3,392, 2,930, 1,756, 1,592, 1,501, 1,432, 1,386, 1,266, 1,122, 1,036, 921, 882, 812, 740 cm^{-1}. ^1H NMR (400 MHz, $CDCl_3$): δ 6.91–6.76 (m, 4H, Ar-H), 5.98–5.92 (m, 3H, Ar-H, O-CH_2-O), 5.56 (d, *J* = 4.1 Hz, 1H, Ar-CH, (C3-phthalide)), 4.41 (d, *J* = 4.1 Hz, 1H, Ar-CH, (C5′-isoquinoline)), 4.32 (d, *J* = 13.9 Hz, 1H, *N*-CH_2*H*), 4.24 (s, 4H, O-CH_2-CH_2-O), 4.17 (d, *J* = 13.9 Hz, 1H, *N*-CH_2*H*), 4.08 (s, 3H, -OCH_3), 3.95 (s, 3H, -OCH_3), 3.84 (s, 3H, -OCH_3), 2.59–2.49 (m, 4H, -C*H*H-*N*-CH_3 (C7′-isoquinoline), *N*-CH_3), 2.36–2.25 (m, 2H, -CH*H*-N-CH_3 (C7′-isoquinoline), Ar-C*H*H (C8′-isoquinoline)), 1.65–1.53 (m, 1H, Ar-CH*H* (C8′-isoquinoline)). ^{13}C NMR (100 MHz, $CDCl_3$): δ 168.0, 152.0, 147.4, 143.3, 142.6, 140.8, 137.1, 135.4, 134.5, 133.7, 124.2, 120.9, 120.5, 120.0, 117.9, 117.7, 117.6, 117.1, 116.4, 100.5, 81.9, 64.2 (x2), 62.1, 60.8, 59.6, 56.6, 50.3, 49.4, 46.0, 22.6. MS (ESI-MS) *m/z*: 576 [*M* + H] + HRMS (ESI): Calcd for $C_{31}H_{33}N_2O_9$ [*M* + H]+: 576.21806, found: 576.21835.

2.10 | Cell culture and reagents

All the chemical reagents and media were obtained from Sigma. Human breast cancer cell line, MCF7 and MDA-MB-231 were obtained from the cell repository of the National Center for Cell Science Pune, Maharashtra, India. The primary breast cancer cells were isolated from the surgically removed tumor tissues of patients. The approval from the Institutional ethical committee of King George's Medical University, Lucknow, Uttar Pradesh, India, and the consent from the patients was taken for the use of samples. Stock solution (100 mM) of the newly synthesized 9-(*N*-arylmethylamino) noscapinoids, **15–17** was prepared with dimethyl sulfoxide (DMSO) and stored at 4°C. The cells were grown at a temperature of 37°C in a 5% CO_2 and 95% humidity in Dulbecco's modified Eagle medium (DMEM, Sigma), supplemented with 10% fetal bovine serum (FBS) and antibiotics. Cells with a 70%–80% confluence were subcultured for bioassays using trypsin-EDTA (0.25%).

2.11 | In vitro cell proliferation assay using MCF-7 and MDA-MB-231 breast cancer cell lines

The cell proliferation assay was performed using MCF7 and MDA-MB-231 human breast cancer cell lines as reported earlier (Naik, Chatterji, et al., 2011; Naik, Santoshi, et al., 2011). In brief, cells were grown in a culture medium (MEM, DMEM) supplemented with 10% FBS, 1% penicillin/streptomycin, 2 mM l-glutamine at 37°C and 5% CO_2. In a 96-well plate, cells were plated at a density of 5×10^3 cells per well and were treated with increasing concentrations (5–100 μM) of noscapine and 9-(*N*-arylmethylamino) noscapinoids, **15–17** for 72 hr. The cells were then stained with 0.4% sulforhodamine B (dissolved in 1% acetic acid). The unbound dye was removed by washing with 1% acetic acid. The protein-bound dye was then extracted with 10 mM Tris base and the absorbance was measured at 564 nm wavelength using a SPECTRAmax PLUS 384 microplate spectrophotometer. The IC_{50} values (the drug concentration required to achieve a cell kill of 50%) of the compounds were determined using the online tool Quest GraphTM IC_{50} Calculator (AAT Bioquest, Inc., https://www.aatbio.com/tools/ic50-calculator).

2.12 | Culture of primary breast tumor cells and in vitro cell proliferation assay

Primary breast tumor cells were isolated from the surgically removed breast tumor tissue of patients (eight nos.) with different stages of breast cancer before drug treatment in aseptic condition. The tumor tissues were treated with 0.25% trypsin and filtered with 70-μm filter followed by centrifugation at 1,073*g* for 3 min with serum-free medium. The filtered cells were collected and plated in T25 flask and incubated with complete DMEM medium, supplemented with 10% FBS and 1% pentrip (mixture of penicillin and streptomycin) at 37°C under 5% CO_2. Fresh media was replaced every 3–4 days, and subsequent passages were performed under the same conditions as mentioned above. The cultured were maintained for homogeneous cell type at sub-confluence between 3 and 8 passages. After the confluence (70% to 80%) reached, the tumor cells were plated at 2,000 cells/well in 96-well plate with standard growth media, DMEM (low glucose). The cells were maintained at 37°C in a humidified atmosphere with 5% CO_2 and were treated with gradient concentrations (5–100 μM) of noscapine and 9-(*N*-arylmethylamino) noscapinoids, **15–17** for 72 hr. Quantification of cells was performed by sulforhodamine B assay, using the CellTiter96 AQueous One Solution Reagent (Sigma). Cells were treated with sulforhodamine B for 30 min, the unbound dye was removed by washing and the bound dye was extracted with 1 mM tris. The absorbance was measured using a SPECTRAmax PLUS 384 microplate spectrophotometer at a wavelength of 564 nm. The percentage of cell survival as a function of drug concentration was plotted and the IC_{50} value was determined using the online tool, AAT Bioquest.

2.13 | Flow cytometry analysis of cell cycle progression

MDA-MB-231 cells were grown in DMEM with 4.5 g/L glucose and L-glutamine supplemented with 10% FBS and 1% penicillin/streptomycin at 37°C in 5% CO_2. Cells were treated with IC_{50} concentration of noscapine and 9-(*N*-arylmethylamino) noscapinoids, **15–17**, dissolved in 1% phosphate buffer saline (PBS) for 72 hr. For the flow cytometer analysis, 2×10^6 cells were harvested and centrifuged; the pellets were washed with ice-cold PBS, and then fixed in 70% ethanol. The cell pellets were centrifuged at 1,000×*g* for 10 min and the pellets were resuspended in 30 μl of phosphate/citrate buffer (0.2 M Na_2HPO_4/0.1 M citric acid, pH 7.5) at room temperature. After 30 min the cell pellets were washed with 5 ml of PBS and incubated with 0.5 ml of propidium iodide (PI; 20 μg/ml in 0.6% Triton-X in PBS) and 0.5 ml of RNase A (20 μg/ml in PBS) for 45 min in dark. Samples were analyzed on a flow cytometer (BD FACS Aria-III) and the progress in the cell cycle was determined.

2.14 | Flow cytometry analysis for apoptosis assay

Apoptosis in cancer cells was detected by Annexin V-FITC detection method by using apoptosis detection kit (Sigma). For experimental purpose 3×10^4 cells per well were seeded on 12 well culture plate and incubated for 24 hr with complete medium. The cells were treated with IC_{50} concentration of noscapine and 9-(*N*-arylmethylamino) noscapinoids, **15–17** for 72 hr. Cells were typsinized and stained with surface marker antibodies (biotin-conjugated Annexin V, FITC-conjugated streptavidin) and PI in 1× binding buffer for 20 min in dark condition at room temperature. Flow cytometer data with 488 nm excitation for PI and emission at 530 nm were collected. Viable cells (Annexin V^-/PI^-), early apoptotic cells (Annexin V^+/PI^-), late apoptotic/necrotic cells (Annexin V^+/PI^+) and late necrotic cells (Annexin V^-/PI^+) were identified and determined their percentage.

2.15 | DAPI staining

Apoptotic cells with the treatment of test compounds were visualized by inverted fluorescence microscopy following DAPI staining. MDA-MB-231 cells were grown

on poly-L-lysine coated coverslips in six-well plates and were treated with noscapine and 9-(*N*-arylmethylamino) noscapinoids, **15–17** at IC_{50} concentration for 72 hr. After incubation, coverslips were fixed in cold methanol and washed with PBS, stained with DAPI, and mounted on slides. Images were captured using an inverted fluorescent microscope (Nikon Eclipse Ts2R-FL). Apoptotic cells were identified by changes in morphology compared to untreated cells.

2.16 | Acridine Orange (AO) & Ethidium bromide (Etbr) staining

MDA-MB-231 cancer cells were grown in culture plates and treated with noscapine and 9-(*N*-arylmethylamino) noscapinoids, **15–17** at IC_{50} concentration for 72 hr. After incubation, coverslips were fixed in cold methanol and washed with PBS. It was stained with acridine orange and ethidium bromide and mounted on slides. Images were captured using an inverted fluorescent microscope (Nikon Eclipse Ts2R-FL). Apoptotic cells were identified by changes in morphology compared to untreated cells.

2.17 | Tubulin purification

Tubulin was purified from the goat brain via temperature cycles and GTP-dependent polymerization and depolymerization (Hamel & Lin, 1981; Panda et al., 2000) using PEM buffer (50 mM pipes, 3 mM $MgSO_4$, and 1 mM EGTA, pH 6.8). The amount of tubulin in the extract was estimated by the Bradford method using BSA as the standard (Bradford, 1976). The purified tubulin was frozen and stored at −80°C for further use.

2.18 | Tubulin-binding assay

Tubulin is autofluorescence in nature due to the presence of several tryptophan amino acids. Therefore, to examine the tubulin-binding of chemical compounds, a fluorescence titration was used to analyze the quenching of the intrinsic fluorescence of tubulin (Dash et al.,). The purified tubulin (2 μM) was treated with 9-(*N*-arylmethylamino) noscapinoids, **15–17** at a concentration of 25 μM in PEM buffer (50 mM pipes, 3 mM $MgSO_4$, 1 mM EGTA, pH 6.8) for 45 min at 35°C. The samples were excited at 295 nm and the emission spectrum was measured at 310–400 nm. For the spectrofluorometric titrations a FlouroMax® 4 spectrofluorometer (Horiba Scientific) assisted by Fluor Essence 3.5 software was used. The experiments were repeated twice.

3 | RESULTS AND DISCUSSION

A battery of noscapine derivatives was developed in past decades to increase the efficacy in inhibiting cancer cell proliferation. Many of these derivatives revealed high tubulin-binding affinity as indicated by lowering the dissociation constant (K_d value) to several folds compared to the lead molecule, noscapine (Aneja et al., 2006b; Jain et al., 2011; Naik et al., 2012; Santoshi et al., 2015). The available experimental data led us to develop a reasonable predictive model for determining the binding affinity of newly designed 9-(*N*-arylmethylamino) noscapinoids and screening of promising derivatives. We are reporting in this study a panel of three 9-(*N*-arylmethylamino) noscapinoids, **15–17** as potent anticancer agents.

3.1 | Molecular docking of designed noscapinoids with tubulin

Noscapinoids, previously reported (Figure 2) and newly designed in this study (Figure 1) were docked onto the binding pocket of noscapinoids (Oliva et al., 2020) and evaluated using a Glide XP_{score} function (Friesner et al., 2004; Halgren et al., 2004). All the noscapinoids were found to docked well within the binding pocket with improved docking score (ranged from −2.038 to −4.492 kcal/mol) compared to noscapine (−1.927 kcal/mol). Further, the best docked poses of each noscapinoid were considered for determining the binding energy with tubulin based on LIE-SGB calculations.

3.2 | Predictive binding affinity of 15–17 with tubulin (LIE-SGB calculation)

The predicted binding energy ($\Delta G_{bind,pred}$) of 9-(*N*-arylmethylamino) noscapinoids with tubulin was determined based on the LIE-SGB empirical prediction model developed in this study by using the experimental activity of training set molecules (Table 1). Different interaction energy terms used in the model were included in Table 1. The values of the coefficients α, β, γ and δ for nonbonding interactions terms U_{vdw}, U_{coul}, U_{rxn} and U_{cav} are 0.08446, −0.00223, −0.000872 and −0.45601, respectively. The largest contribution for the binding free energy comes from the van der Waals interactions. The predicted binding energy ($\Delta G_{bind,pred}$) of the training set molecules based on the LIE-SGB model is very close to the experimental binding energy ($\Delta G_{bind,expt}$; root mean square error was 0.223 kcal/mol). The accuracy of the prediction model is determined from the value of the squared correlation coefficient ($R^2 = 0.998$) and analysis of variance (F-value = 3,742.6).

$$\Delta G_{bind,pred} = 0.08446 < U_{vdw} > - 0.00223 < U_{coul} > - 0.00872 < U_{rxn} > - 0.45601 < U_{cav} > .$$

($n = 11$, $R^2 = 0.998$, $s = 0.243$, $F = 3{,}742.6$, $p \leq .001$).

The LIE-SGB model was used to predict the $\Delta G_{\text{bind,pred}}$ of the newly designed 9-(*N*-arylmethylamino) noscapinoids. The top three 9-(*N*-arylmethylamino) noscapinoids (Figure 3) that revealed improved $\Delta G_{\text{bind,pred}}$ of −6.694 kcal/mol for **15**, −7.118 kcal/mol for **16** and −7.732 kcal/mol for **17**, in comparison to noscapine (−5.135 kcal/mol) were screened out for chemical synthesis and experimental evaluation. All the three compounds also have improved docking score (−3.941 kcal/mol for **15**, −4.175 for **16** and −4.208 for **17**).

3.3 | MD simulations and prediction of predicted binding free energy using MM-PBSA

The docked complexes of 9-(*N*-arylmethylamino) noscapinoids, **15–17** with tubulin were used to perform MD simulations of 100 ns to observed their stability, followed by MM-PBSA calculation to determine their predicted binding energy ($\Delta G_{\text{bind,pred}}$). The convergence of the MD trajectories was monitored by plotting root mean square deviation (RMSD) and radius of gyration (Rg) of the backbone C_α atoms with respect to time. The RMSD and the Rg values were very small after ~40 ns suggesting the stability of the system (Figures S11 and S12). It was also observed that the root mean square fluctuations (RMSF) of most of the residues of tubulin in the bound form with ligands and in the free form were not so much different (within the range of 1 to 2.5 Å) indicating that the residues were more rigid. However, only very few residues showed fluctuation >5 Å, indicating that these residues seem to be more flexible (Figure S13). All the three 9-(*N*-arylmethylamino) noscapinoids, **15–17** were found to accommodate well inside the binding cavity (Figure 5) at the interface between α- and β-tubulin. However, their binding modes inside the binding cavity are distinct as shown in the ligplot may be due to different functional groups (Figure 6). As shown in the figure the most potent 9-(*N*-arylmethylamino) noscapinoid **17** in terms of binding energy and docking score interacts more intensely with the residues of tubulin compared to the other two derivatives. Its binding involved four hydrogen bonds (dashed line). The oxygen atom O10 hydrogen bonded with the side chain nitrogen atom (ND2) of residue Asn A228 (bond length 3.04 Å), the nitrogen

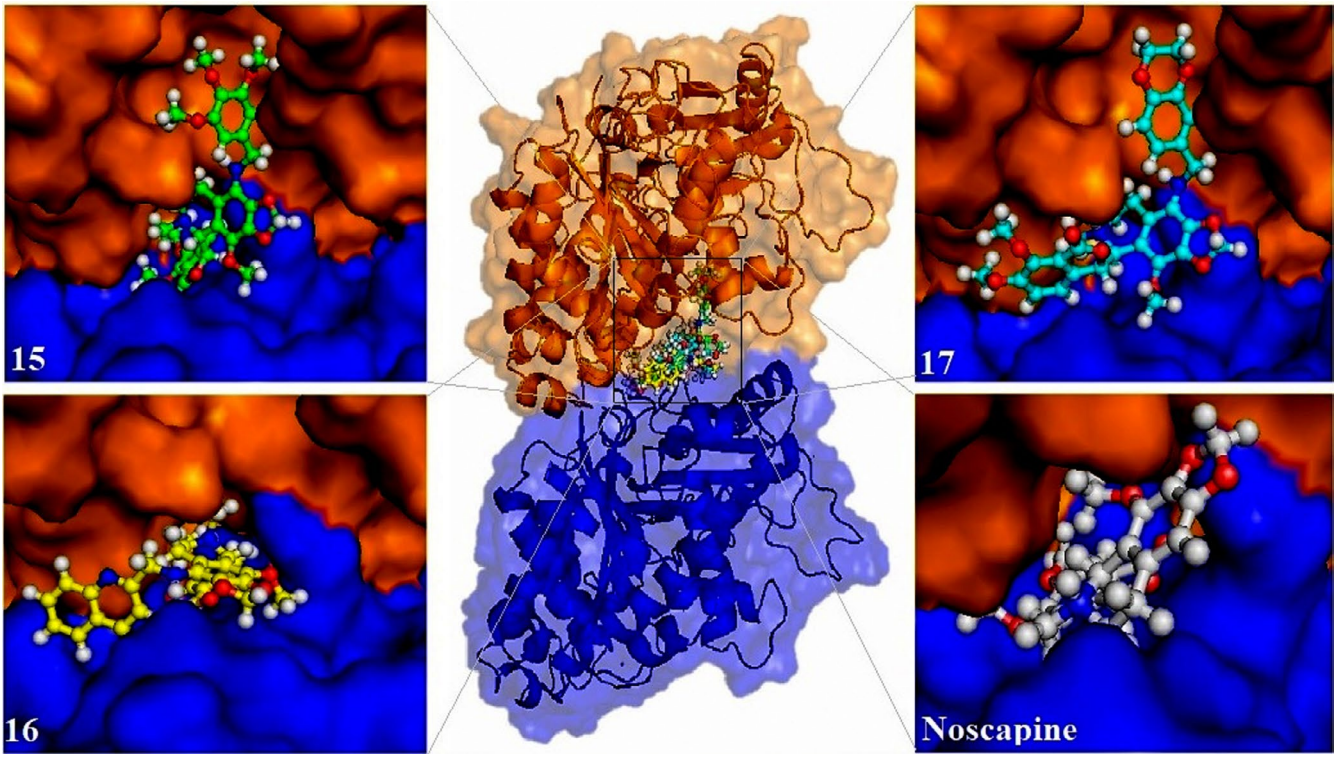

FIGURE 5 The newly designed 9-(*N*-arylmethylamino) noscapinoids, **15–17** are well accomodated inside the noscapine binding site at the interface of α- and β-tubulin. The binding site is represented as macromodel surface according to α- and β-tubulin (α-tubulin is represented in blue color and β-tubulin is represented in brown color)

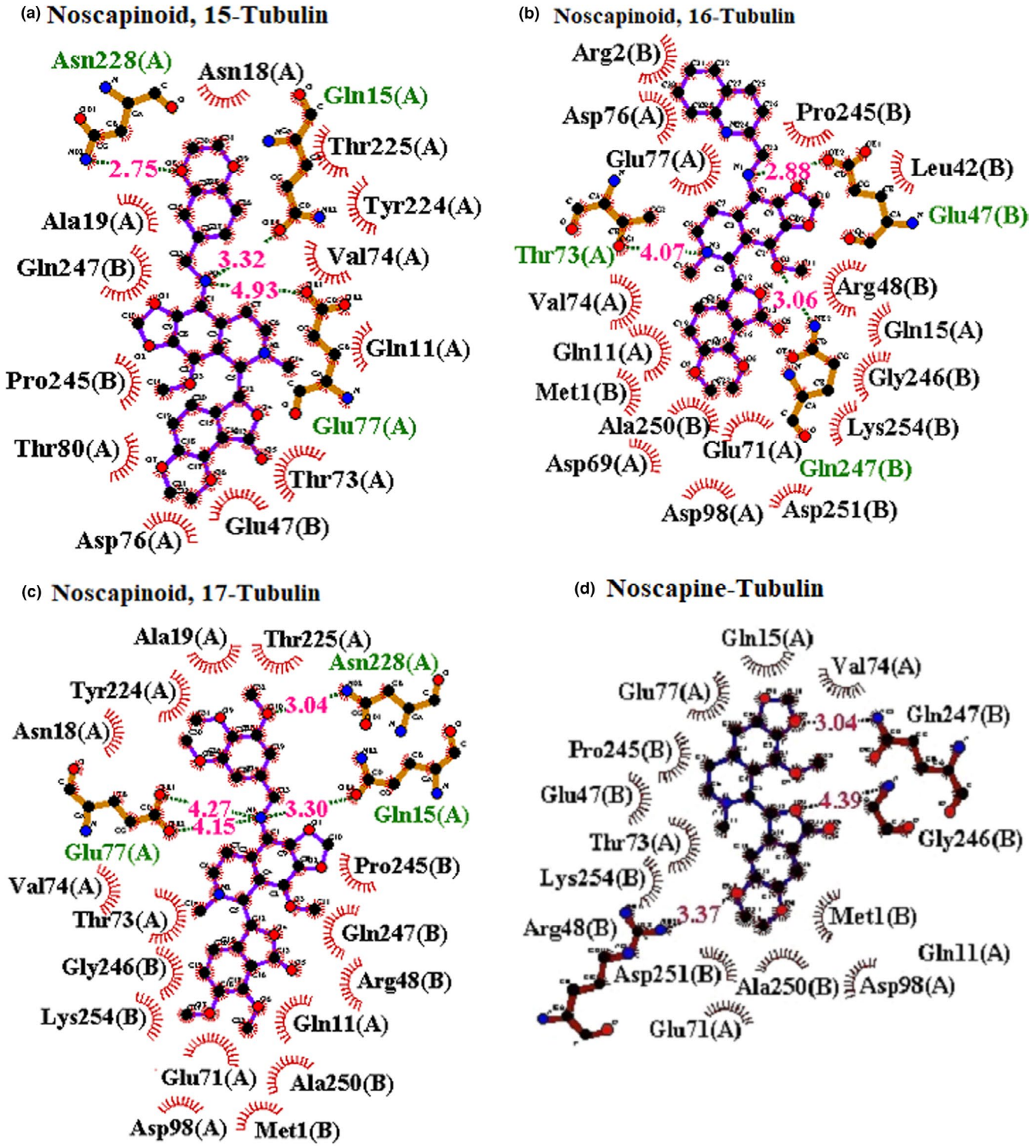

FIGURE 6 Two dimensional representation of interaction observed between the binding site residues of tubulin with 9-(*N*-arylmethylamino) noscapinoids, (a) **15**, (b) **16**, (c) **17** and (d) Noscapine. Dashed lines denote hydrogen bonds and numbers indicate hydrogen bond lengths in Å. Hydrophobic interactions are shown as arcs with radial spokes. The figure was made using LIGPLOT. The residues within 5 Å distance from the docked ligands were only shown in the figures

atom (N1) form 03 hydrogen bonds with side chain oxygen atom (OE_2) of Glu A77 (bond length 4.15 Å), OE1 of Glu A77 (bond length 4.27 Å) and OE1 of Gln A15 (bond length 3.3 Å; Figure 6c). In contrast, the binding of 9-(*N*-arylmethylamino) noscapinoids, 15 and 16 involved only three hydrogen bonds with the binding site residues (Figure 6a,b). In case of molecule **15**, the oxygen atom O8 hydrogen bonded with the side chain nitrogen

TABLE 2 Binding free energy and its components (kcal/mol) for noscapine and its 9-*N*-arylmethylamino derivatives, **15–17** with the receptor αβ tubulin dimmer

Energy components (kcal/mol)	Noscapine	15	16	17
ΔE_{vdw}	−56.22	−32.64	−35.91	−57.90
ΔE_{ele}	−202.5	−184.3	−177.3	−190.6
$\Delta G_{solv,PB}$	108.6	52.48	47.45	76.26
$\Delta G_{sol\text{-}np}$	−6.19	−4.28	−4.74	−6.38
$\Delta G_{bind,\ PBSA}$	−156.3	−167.4	−170.5	−178.6

TABLE 3 Hydrogen bonding energy contribution of binding site amino acids of αβ tubulin dimmer for the binding of noscapine and its 9-*N*-arylmethylamino derivatives

Binding site residues	Hydrogen bonding energy contribution (kcal/mol)			
	Noscapine	15	16	17
Gln 247(B)	−0.493	—	−0.462	—
Arg 48(B)	−0.262	—	—	—
Asn 228(A)	—	−0.463	—	−0.482
Gln 15(A)	—	−0.402	—	−0.452
Glu 47(B)	—	—	−0.436	—

Note: The hydrogen bonds with a distance of ≤3.6 Å are only considered for the calculation.

atom (ND2) of residue Asn A228 (bond length 2.75 Å), the nitrogen atom N1 form two hydrogen bonds with side chain oxygen atoms (OE1) of Glu A77 (bond length 4.93 Å) and Gln A15 (bond length 3.32 Å). Similarly in case of molecule **16**, the oxygen atom (O3) hydrogen bonded with the side chain nitrogen atom (NE2) of Gln B247 (bond length 3.06 Å), the nitrogen atom (N1) form hydrogen bond with the side chain oxygen atom (OE2) of residue Glu B47 (bond length 2.88 Å) and the nitrogen atom (N3) hydrogen bonded with the side chain oxygen atom (OG1) of residue Thr A73 (bond length 4.07 Å). Besides, hydrogen bonding, a good number of hydrophobic interactions were involved in the binding of 9-(*N*-arylmethylamino) noscapinoids **15–17** with binding site residues (Tables S14–S17). Inspired by our computational findings, we have chemically synthesized the newly designed -(*N*-arylmethylamino) noscapinoids **15–17** to further evaluate their anticancer potential.

The predictive binding free energy ($\Delta G_{bind,pred}$) of noscapine and its 9-(*N*-arylmethylamino) noscapinoids, **15–17** based on MM-PBSA is collated in Table 2. It is revealed that the 9-(*N*-arylmethylamino) noscapinoids, **15–17** have high $\Delta G_{bind,pred}$ (ranges from −167.4 kcal/mol to −178.6 kcal/mol) compared to noscapine (−156.3 kcal/mol). Both the intermolecular van der Waals (ΔE_{vdw}) and the electrostatic (ΔE_{ele}) interactions were found to be significant contributors to the binding energy. Also, the nonpolar solvation terms ($\Delta G_{sol\text{-}np}$), which define the burial of solvent accessible surface area upon binding was somewhat favorable to the binding of ligands. In contrast, the polar solvation terms (ΔG_{PB}) and the electrostatic interaction energy ($\Delta G_{ele,PB}$) were not favorable to the binding of ligands. This might be due to the large desolvation penalty of charged and polar groups. The hydrogen bonding energy contribution of binding site amino acids for the binding of the noscapine and its 9-*N*-arylmethylamino derivatives is included in Table 3. The hydrogen bonding energy contribution was found to be high for 9-*N*-arylmethylamino noscapinoids, **17** compared to 16 and 15.

3.4 | *N*-alkyl amine-noscapinoids 15–17 inhibits proliferation of MCF-7 and MDA-MB-231

Based on our in silico results, we next want to test if the 9-(*N*-arylmethylamino) noscapinoids, **15–17,** affected proliferation of breast cancer cell lines, MCF-7 and MDA-MB-231. *N*-arylmethylamino-noscapinoids, **15–17** exhibited potent cytotoxic activity in comparison to noscapine using both the cell lines (Figure 7). The IC_{50} values for the test compounds for both the cell lines are collated in Table 4. The IC_{50} value amounted to 62.2, 11.2, 8.03 and 3.8 μM for noscapine, **15**, **16** and **17**, respectively for MCF-7 cells. Parenthetically, a similar modest IC_{50} value of 59.8, 24.4, 9.7 and 6.4 μM was measured for noscapine, **15**, **16** and **17**, respectively for MDA-MB-231 cells.

3.5 | 9-(*N*-arylmethylamino) noscapinoids, 15–17 inhibits proliferation of primary breast tumor cells

We next wanted to evaluate whether the newly developed 9-(*N*-arylmethylamino) noscapinoids, **15–17** also inhibit the proliferation of primary breast tumor cells. We have obtained the surgically removed breast tumor samples from 08 different patients with different stages of breast cancer and isolated the primary cancer cells. The IC_{50} values for the test compounds are collated in Table 5. The IC_{50} value ranges from 41.8 to 51.5 μM for noscapine, 21.3 to 32.2 μM for **15**, 9.9 to 16.9 μM for **16** and 3.2 to 8.7 μM for **17** using a panel of primary breast tumor cells (Table 3). All the *N*-arylmethylamino-noscapinoids developed exhibited potent cytotoxic activity in comparison to noscapine using all the primary breast cancer cells (Figure 8).

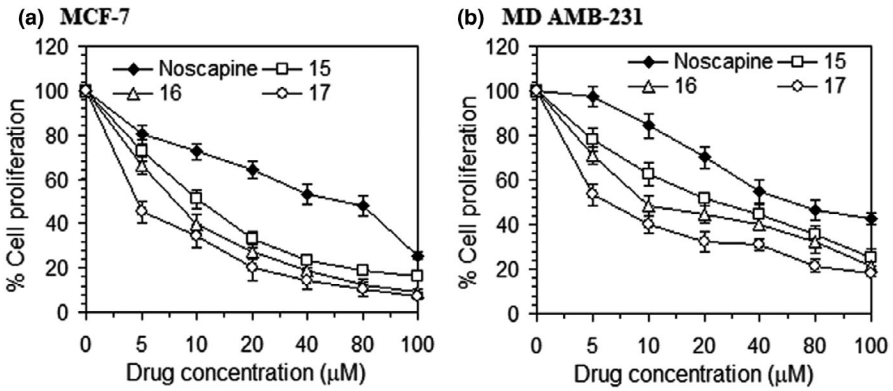

FIGURE 7 The 9-(*N*-arylmethylamino) noscapinoids, **15–17** are more active compared to noscapine in inhibiting the proliferation of human breast cancer cells. Both (a) MCF-7 and (b) MDA-MB-231cells were treated with noscapine and its 9-(*N*-arylmethylamino) noscapinoids, **15–17** for 72 hr. Each value represents the average of three independent experiments

TABLE 4 IC_{50} values of novel 9-(*N*-arylmethylamino) noscapinoids, **15–17** using two human breast adenocarcinoma cell lines, MCF-7 and MDA-MB-231

IC_{50} (μM)				
	Noscapine	15	16	17
MCF-7	44.3 ± 3.9	11.2 ± 2.5	7.9 ± 1.7	3.9 ± 0.8
MDA-MB-231	58.4 ± 4.8	24.9 ± 2.9	14.8 ± 1.4	5.4 ± 1.2

Note: All the novel derivatives were found to have improved antiproliferative activity compared to noscapine.

TABLE 5 IC_{50} values of novel 9-(*N*-arylmethylamino) noscapinoids, **15–17** using primary breast tumor cells isolated from breast tumor tissue of different patients

IC_{50} (μM)				
Primary breast tumor cells	**Noscapine**	15	16	17
1	51.5 ± 5.7	32.2 ± 4.3	16.5 ± 2.4	7.9 ± 1.2
2	44.2 ± 4.9	25.6 ± 3.9	13.4 ± 2.9	5.1 ± 0.8
3	42.3 ± 5.3	20.9 ± 3.5	10.4 ± 2.3	4.1 ± 0.6
4	38.2 ± 5.5	24.8 ± 4.2	12.5 ± 1.9	7.6 ± 1.3
5	41.8 ± 4.7	27.4 ± 3.4	11.8 ± 3.1	4.7 ± 1.5
6	46.8 ± 4.9	22.3 ± 3.7	10.1 ± 2.8	3.2 ± 0.6
7	43.3 ± 5.3	21.3 ± 2.8	9.9 ± 1.9	6.1 ± 0.5
8	50.4 ± 4.2	30.8 ± 2.6	16.9 ± 1.6	8.7 ± 0.8

Note: All the novel derivatives were found to have improved antiproliferative activity compared to noscapine.

3.6 | *N*-arylmethylamino-noscapinoids induced apoptosis to cancer cells

The induction of apoptotic cell death to breast cancer cell with the treatment of *N*-alkyl amine-noscapinoids was investigated by FACS using fluorescent dyes, annexin V and PI. The phosphatidylserine translocated to outer leaflet of cell membrane during apoptosis is labelled with annexin V. In contrast, the DNA-binding fluorescent dye, PI intercalates with the DNA when the cells are undergone apoptosis. Thus the apoptotic cells are quantified to large extent using both the dyes by FACS analysis. The percentage of early and late apoptotic cells using MDA-MB-231 cell lines for the treatment of noscapine and its *N*-alkyl amine-noscapinoids, **15–17** with IC_{50} concentration for 72 hr is collated in Table 6. Representative figures of flow cytometry analysis are included in Figure 9. After 72 hr, the control untreated cell culture contained only very few early apoptotic (3.5%) and late apoptotic cells (2.0%), which were considered as the background cell death due to regular trauma during cell culture (Table 5). However, the percentage of early apoptotic cells of 20%, 15%, 15%, and 6% as well as late apoptotic cells of 25%, 30%, 40% and 24% with treatments of noscapine and its *N*-alkyl amine-noscapinoids, **15–17**, respectively were found to be significantly high compared to controlled untreated cells (Table 6).

Besides, morphological examination using DAPI, Acridyne orange and Ethidium bromide staining revealed apoptotic cell death of MDMB-231 cancer cells characterized by condensed chromatin, formation of membrane blebs and numerous fragmented nuclei (Figures 10 and 11).

3.7 | Interference in cell cycle progression by 9-(*N*-arylmethylamino) noscapinoids

The effect of noscapine and 9-(*N*-arylmethylamino) noscapinoids, **15–17** (25 μM concentration) on the cell cycle progression of MDA-MB-231 based on FACS analysis and represented in Figure 12. Accumulation of fluorescently labelled DNA in presence of noscapinoid, demonstrates the perturbation of cell cycle and cell death. The presence of 2N DNA indicates that the cells are in the G1 phase, while the accumulation of duplicated 4N DNA indicates that the cells are in G2 and M phases. Accumulation of DNA in between 2N and 4N peaks represents, the cells are in the S phase. In contrast, less than 2N DNA indicates the apoptotic cells in

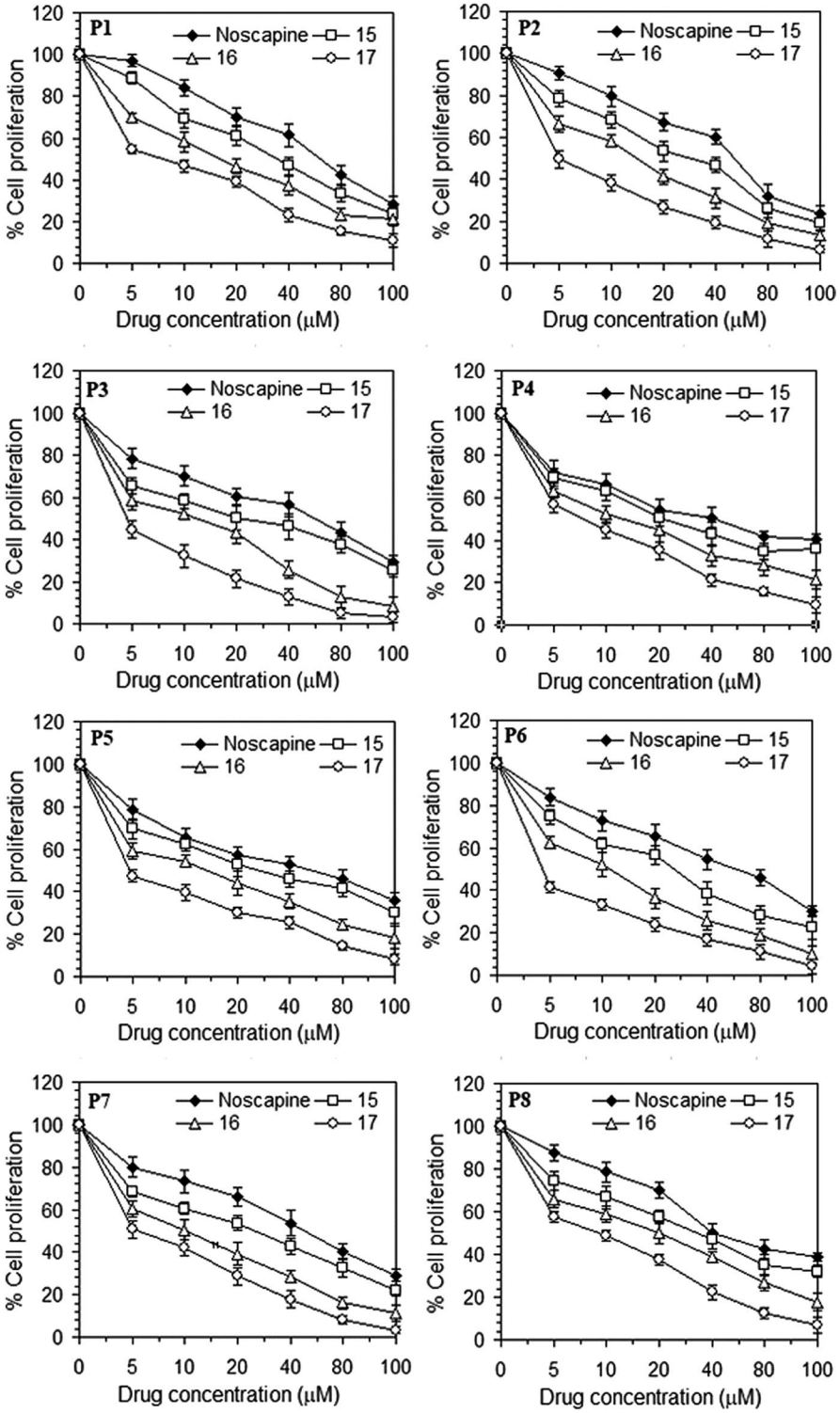

FIGURE 8 The 9-(*N*-arylmethylamino) noscapinoids, **15–17** are more active compared to noscapine in inhibiting the proliferation of a panel of human primary breast tumor cells. All the cells treated with **15–17** for 72 hr. Each value represents the average of three independent experiments

Viability/Apoptotic	Control (%)	Noscapine (%)	15 (%)	16 (%)	17 (%)
Q1	3.5	20	15	15	6
Q2	2	25	30	40	24
Q3	94	50	53	42	32.4
Q4	0.5	5	2	3	37

TABLE 6 Percentage of early apoptotic (Q1), late apoptotic (Q2), viable (Q3) and necrotic (Q4) cells with the treatment of 9-(*N*-arylmethylamino) noscapinoids, **15–17** measured by flow cytometry

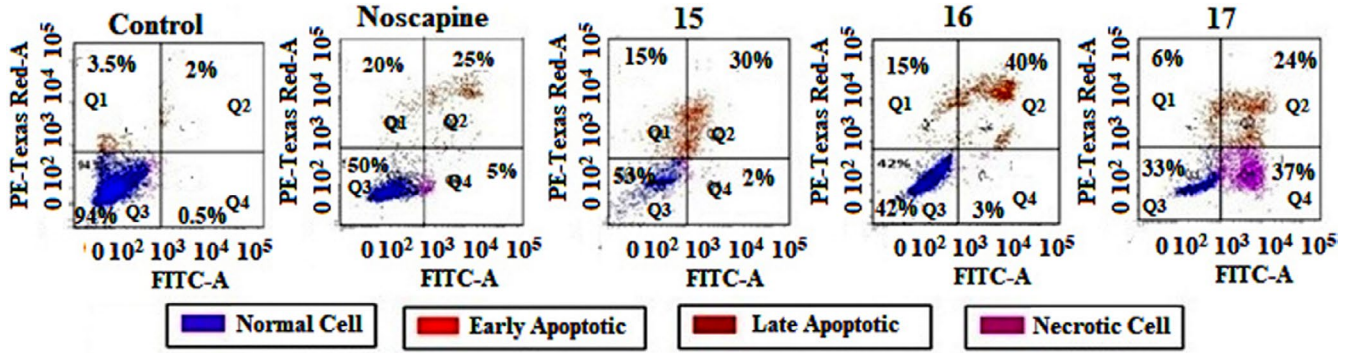

FIGURE 9 Flow cytometry analysis of phosphatidylserine (PS) exposure in MDA-MB-231 cells treated with noscapine and its 9-(*N*-arylmethylamino) noscapinoids, **15–17** with IC_{50} concentration for 72 hr and compared with non treated control cells. Annexin-V was used, in combination with the non-vital dye propidium iodide (PI), to distinguish among three sub-populations: PI-negative and Alexa Fluor 488-negative viable cells with intact membrane and preserved amino-phospholipid asymmetry (PI-, Alexa Fluor 488-), PI-negative and Alexa Fluor 488-positive early apoptotic cells with intact cellular membrane exposing PS (PI-, Alexa Fluor 488+), and PI-positive and Alexa Fluor 488-positive late apoptotic cells with compromised asymmetry and membrane permeability (PI+, Alexa Fluor 488+). Representative results of three independent experiments

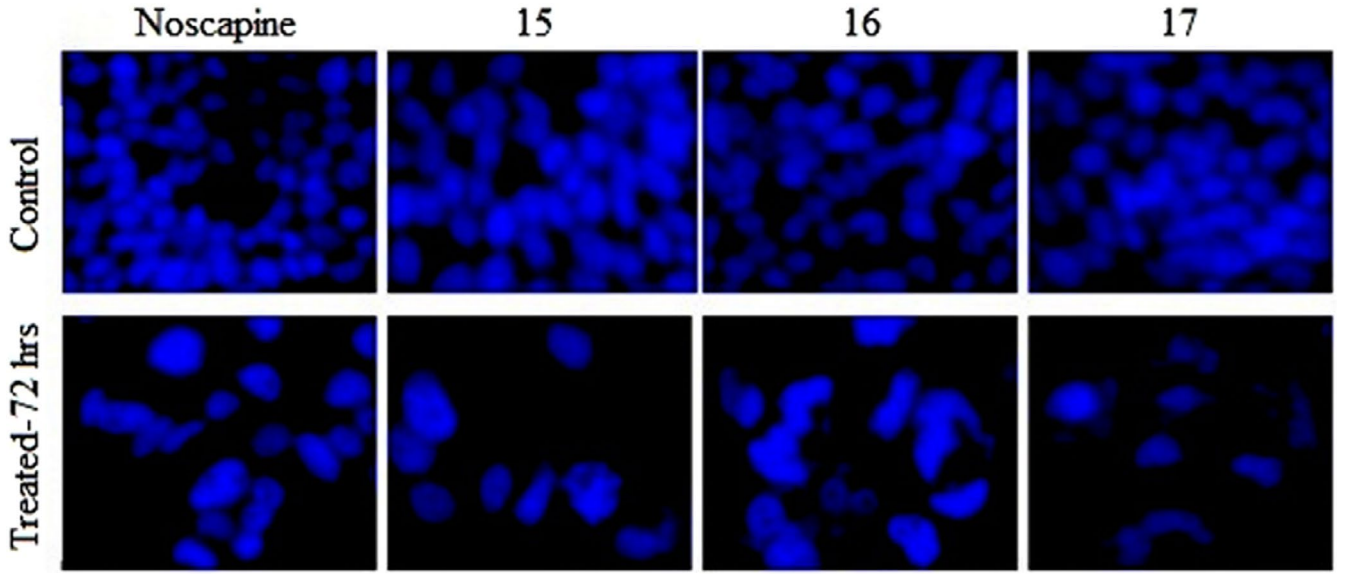

FIGURE 10 The changes in morphological characters such as chromatin condensation, plasma membrane blebbing and appearance of small, apoptotic bodies indicated the apoptotic cells. Panels show morphological features of cells stained with DAPI from control cells (upper panels) and cells treated with IC_{50} concentration of noscapine and 9-(*N*-arylmethylamino) noscapinoids, **15–17** (lower panels) for 72 hr using fluorescence microscopy. The apoptotic cancer cells were evident after 72 hr of drug treatment

which the DNA is degraded to different extents. Treatment of MDA-MB-231 cells for 72 hr with the noscapine and 9-(*N*-arylmethylamino) noscapinoids, **15–17** led to significant inhibition of the cell cycle profile at IC_{50} concentration. FACS analysis revealed a high accumulation of cells in the G2/M phase at 72 hr of treatment with the test compounds (Table 7). In contrast to G2/M block, a hypodiploid DNA content peak (sub-G1) was seen to rise at 72 hr of drug treatment, indicating dying cells.

3.8 | 9-(*N*-arylmethylamino) noscapinoids, 15–17 binds to tubulin at high affinity

Microtubules are autofluorescent by nature due to the presence of aromatic amino acids, tryptophan which can be selectively measured by exciting at 295 nm. Any chemical compounds that bind with tubulin and alter its conformation lead to a decrease in its intrinsic fluorescence. This is a standard assay to test whether a chemical compound binds to tubulin or not. We have used a similar assay to test whether the 9-(*N*-arylmethylamino) noscapinoids, **15–17** also bind to tubulin or not. It was revealed

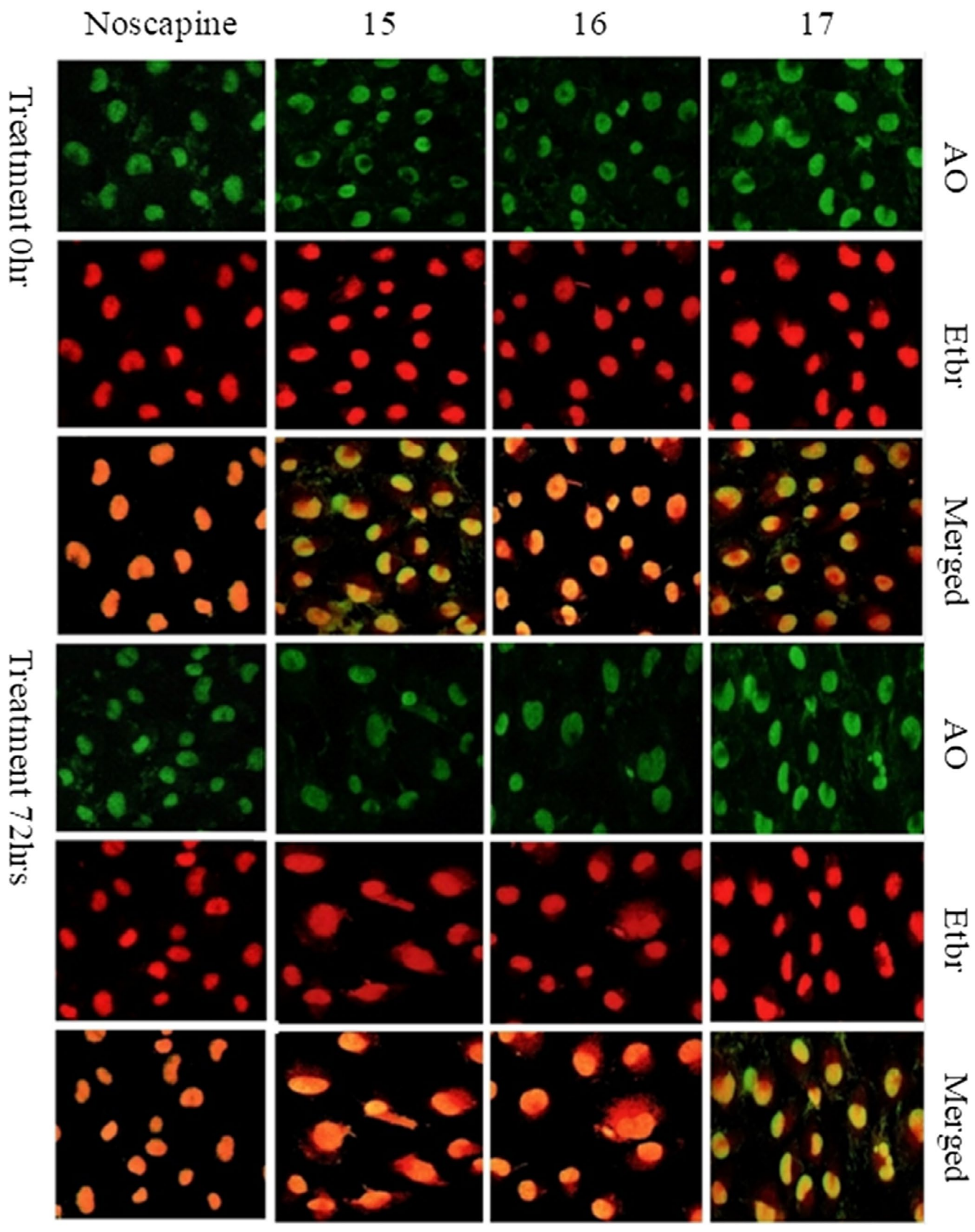

FIGURE 11 The changes in morphological characters such as chromatin condensation, plasma membrane blebbing and appearance of small, apoptotic bodies indicated the apoptotic cells. Panels show morphological features of cells stained with AO, EtBr and merged channel of AO and EtBr from 0h treatment (upper panels) and cells treated with IC_{50} concentration of noscapine and 9-(*N*-arylmethylamino) noscapinoids, **15–17** (lower panels) for 72 hr using fluorescence microscopy. The apoptotic cancer cells were evident after 72 hr of drug treatment

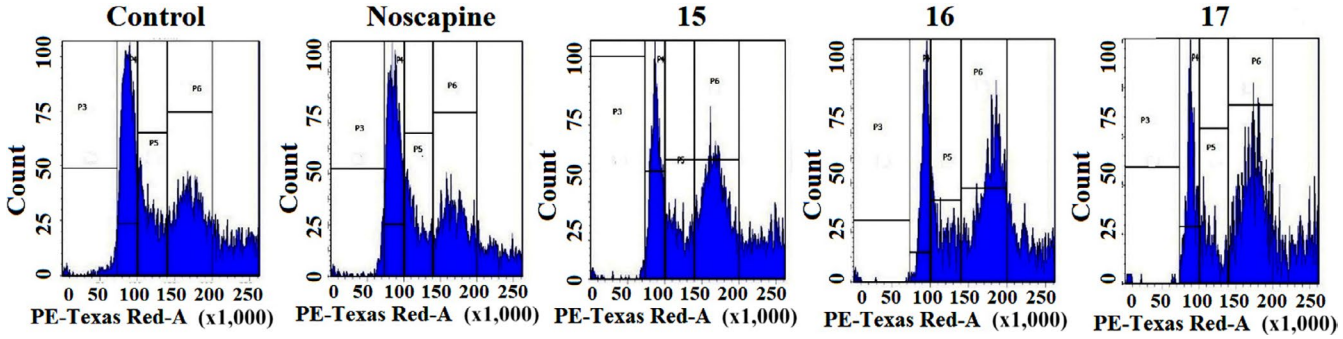

FIGURE 12 Noscapine and its 9-(*N*-arylmethylamino) noscapinoids, **15–17** perturb cell cycle progression at G2/M phase followed by the appearance of a hypodiploid (sub-G1) DNA peak that indicate apoptotic cells. Panels a–e demonstrated the analyses of cell cycle progression, determined by flow cytometry in MDA-MB-231 cells treated with IC_{50} concentration of noscapine and its *N*-alkyl-amine derivatives for 72 hr

TABLE 7 Effect of noscapine and its 9-(*N*-arylmethylamino) noscapinoids, **15–17** on cell cycle progression of MDA-MB-231 cells treated with IC_{50} concentration for 72 hr before being stained with propidium iodide for cell cycle analysis

	72 hr			
	Sub-G_1	**G_0/G_1**	**S**	**G_2/M**
Control	0.7	21	23.4	10.4
Noscapine	6.4	17.5	13.4	26.5
15	9.8	15.8	14.2	28.1
16	13.2	17.2	10.1	31.3
17	18.5	15.3	13.4.	32.7

that intrinsic fluorescence of tubulin, decreased in presence of 9-(*N*-arylmethylamino) noscapinoids, **15–17,** suggests the binding capability of these compounds to tubulin. The relative percentage of decrease in fluorescence intensity was 5.034%, 14.094% and 22.148% respectively in presence of 25 μM concentration of **15–17** (Figure 13), compared to control.

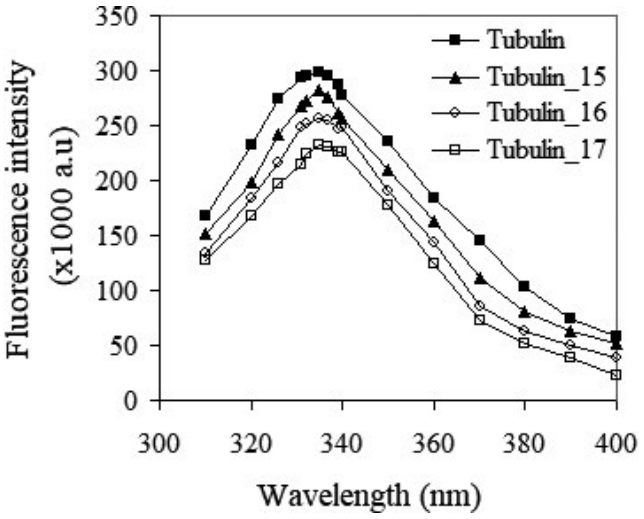

FIGURE 13 Treatment of purified tubulin with 9-(*N*-arylmethylamino) noscapinoids, **15–17** at a concentration of 25 μM quenched the intrinsic fluorescence of tubulin significantly compared to untreated tubulin. The relative percentage of decreased in fluorescence intensity was 5.034%, 14.094% and 22.148% respectively in presence of 25 μM concentration of **15–17** compared to control. Emission spectra were collected in a range of 310–400 nm

4 | DISCUSSION

Microtubule-targeting drugs are widely employed in the clinic to treat different types of cancer. Mostly, three classes of drugs namely, taxanes, vinca alkaloids and colchicine analogs are well recognized and the sites they positioned on the tubulin, have been well studied (Jordan & Wilson, 2004). Traditionally, these classes of drugs either stabilize microtubules, causing over polymerization of microtubules into bundles and sheets, such as the taxane family or destabilizes microtubules resulting in depolymerization of microtubules into soluble tubulin, like the vinca alkaloids. Unfortunately, the clinical success of these drugs has been severely hampered by the emergence of various toxicities, such as gastrointestinal toxicity, alopecia, and peripheral neuropathy. A coupled aspect of the toxicity manifestation is their lack of specificity for dividing cells. Moreover, patients have developed resistance to these drugs. Yet another class of microtubule-binding anticancer agents is based upon noscapine, a non-sedative, naturally occurring opium alkaloid and is known for its antitussive properties for decades (Ye et al., 1998; Zhou et al., 2005). Ever since, noscapine has been successfully shown to inhibit various neoplasms in vitro as well as in vivo such as leukemia and lymphoma (Ke et al., 2000; Sung et al., 2010; Ye et al., 1998), melanoma (Landen et al., 2002), ovarian (Zhou, Gupta, et al., 2002), gliomas (Landen et al., 2004), breast (Aneja et al., 2006), lung (Jackson et al., 2008), and colon (Aneja, Dhiman, et al., 2007; Aneja, Ghaleb, et al., 2007) cancer. It was

demonstrated that noscapine and its analogs, collectively referred to as the noscapinoid family, do not impair crucial microtubule functions mainly by maintaining the steady-state equilibrium between the monomeric and polymeric form of tubulin (Karna et al., 2011). As a result, this class of microtubule-interfering agents escapes the severe side effects of currently available tubulin-binding chemotherapeutics. Hence, noscapine derivatives can potentially be exploited for therapeutic usage individually or in combination with existing toxic anti-microtubule drugs.

Ongoing efforts of rational design and chemical synthesis to improve the therapeutic efficacy and pharmacological properties of noscapine have yielded a battery of noscapine derivatives (Aneja et al., 2006a, 2006b, 2006c, 2006d; Manchukonda et al., 2013, 2014; Meher et al., 2021; Naik, Chatterji, et al., 2011; Naik, Santoshi, et al., 2011; Santoshi et al., 2015). These derivatives have been extensively shown to impede cell cycle progression, inhibit cell proliferation and induce apoptosis in a variety of cancer cells both in vitro and in xenograft models of human cancers implanted in nude mice (Aneja, Dhiman, et al., 2007; Aneja, Ghaleb, et al., 2007; Aneja et al., 2006e, 2008). From a synthetic perspective, most of these derivatives were generated by the chemical manipulation of the C-9 position on the isoquinoline ring system of noscapine. The C-9 substituted derivatives of noscapine revealed superior activity (Aneja et al., 2006a, 2006b). In particular the 9-bromo-noscapine is well-studied because of its effectiveness against drug-resistant xenograft tumors without any detectable toxicity (Aneja et al., 2006e, 2008). This strongly suggested that chemical maneuvering at the C-9 position had a significant impact on the anticancer activity of the parent molecule. Based upon this impetus, we have rationally designed a new series of derivatives of noscapine by substituting alkyl or arylalkyl units at C-9 position to examine their anticancer potential. Finally based on our in silico efforts we have screened out three 9-(*N*-arylmethylamino) noscapinoids, **15–17** based on their lowest negative docking score and predictive binding free energy for chemical synthesis and experimental validation.

All three synthesized 9-(*N*-arylmethylamino) noscapinoids, **15–17** showed antiproliferative activity at a lower concentration compared to the parent compound against two human breast cancer cell lines, MCF-7 and MDA-MB-231 as well as a panel of primary breast tumor cells. It is also revealed that each compound has a narrow range of antiproliferative activity among these cells. These differences in cellular sensitivities to the same compound may be due to altered expression of β-tubulin isotypes, or point mutations in tubulin resulting in alterations of expression patterns of post-translational modifications of tubulin regulatory proteins, such as stathmin, microtubule-associated protein (MAP), tau and MAP4 (Burkhart et al., 2001; Cabral et al., 1982). These changes in microtubule accessory proteins have been well recognized to affect microtubule dynamicity and can perhaps contribute to the development of drug resistance (Liu et al., 2001). Furthermore, these derivatives significantly arrest cells at the G2/M phase of the cell cycle followed by apoptotic cell death, as revealed by several prototypic features of apoptosis. Therefore, these novel compounds may prove efficacious not only in the treatment of breast carcinoma but also for other types of cancers. Our results compel us to continue to examine the effects of these novel compounds on in vivo animal experiments with the final goal of taking it to the human clinical study.

ACKNOWLEDGMENTS

We would like to acknowledge the financial support provided by the Indian Council of Medical Research (Grant No. 5/13/13/2019/NCD_III), Govt. of India. Rajesh Kumar Meher wishes to acknowledge the award of student research fellowship (DST/INSPIRE/Code No.: IF160351). We are also grateful to Satyandra Kumar Singh, Center for Advance Research, Stem Cell and Tissue Culture Laboratory, King George's Medical University for providing extended facilities to test the compounds with primary breast tumor cells.

CONFLICT OF INTEREST

The authors declare that they have no know competing financial interests or personal relationships that could have appeared to influence the work reported in this paper.

DATA AVAILABILITY STATEMENT

Data sharing is not applicable to this article as no new data were created or analyzed in this study.

ORCID

Srinivas Kantevari https://orcid.org/0000-0003-4270-9651

REFERENCES

Abraham, M. J., Murtola, T., Schulz, R., Páll, S., Smith, J. C., Hess, B., & Lindahl, E. (2015). GROMACS: High performance molecular simulations through multi-level parallelism from laptops to supercomputers. *SofwareX*, *1*, 19–25. https://doi.org/10.1016/j.softx.2015.06.001

Aneja, R., Dhiman, N., Idnani, J., Awasthi, A., Arora, S. K., Chandra, R., & Joshi, H. C. (2007). Preclinical pharmacokinetics and bioavailability of noscapine, a tubulin-binding anticancer agent. *Cancer Chemotherapy and Pharmacology*, *60*, 831–839. https://doi.org/10.1007/s00280-007-0430-y

Aneja, R., Ghaleb, A. M., Zhou, J., Yang, V. W., & Joshi, H. C. (2007). p53 and p21 determine the sensitivity of noscapine-induced apoptosis in colon cancer cells. *Cancer Research*, *67*, 3862–3870. https://doi.org/10.1158/0008-5472.CAN-06-4282

Aneja, R., Liu, M., Yates, C., Gao, J., Dong, X., Zhou, B., Vangapandu, S. N., Zhou, J., & Joshi, H. C. (2008). Multidrug resistance-associated protein overexpressing teniposide-resistant human lymphomas

undergo apoptosis by a tubulin-binding agent. *Cancer Research*, *68*, 1495–1503. https://doi.org/10.1158/0008-5472.CAN-07-1874

Aneja, R., Lopus, M., Zhou, J., Vangapandu, S. N., Ghaleb, A., Yao, J., Nettles, J. H., Zhou, B., Gupta, M., Panda, D., Chandra, R., & Joshi, H. C. (2006c). Rational design of the microtubule-targeting anti-breast cancer drug EM015. *Cancer Ressearch*, *66*, 3782–3791. https://doi.org/10.1158/0008-5472.CAN-05-2962

Aneja, R., Vangapandu, S. N., & Joshi, H. C. (2006d). Synthesis and biological evaluation of a cyclic ether fluorinated noscapine analog. *Bioorganic & Medicinal Chemistry*, *14*, 8352–8358. https://doi.org/10.1016/j.bmc.2006.09.012

Aneja, R., Vangapandu, S. N., Lopus, M., Chandra, R., Panda, D., & Joshi, H. C. (2006a). Development of a novel nitro-derivative of noscapine for the potential treatment of drug-resistant ovarian cancer and T-cell lymphoma. *Molecular Pharmacology*, *69*, 1801–1809. https://doi.org/10.1124/mol.105.021899

Aneja, R., Vangapandu, S. N., Lopus, M., Viswesarappa, V. G., Dhiman, N., Verma, A., Chandra, R., Panda, D., & Joshi, H. C. (2006b). Synthesis of microtubule-interfering halogenated noscapine analogs that perturb mitosis in cancer cells followed by cell death. *Biochemical Pharmacology*, *72*, 415–426. https://doi.org/10.1016/j.bcp.2006.05.004

Aneja, R., Zhou, J., Zhou, B., Chandra, R., & Joshi, H. C. (2006e). Treatment of hormone-refractory breast cancer: Apoptosis and regression of human tumors implanted in mice. *Molecular Cancer Therapy*, *5*, 2366–2377. https://doi.org/10.1158/1535-7163.MCT-06-0205

Berendsen, H. J., van der Spoel, D., & van Drunen, R. (1995). GROMACS: A message-passing parallel molecular dynamics implementation. *Computer Physics Communication*, *91*, 43–56. https://doi.org/10.1016/0010-4655(95)00042-E

Bradford, M. M. (1976). A rapid and sensitive method for the quantitation of microgram quantities of protein utilizing the principle of protein-dye binding. *Analytical Biochemistry*, *72*, 248–254. https://doi.org/10.1006/abio.1976.9999

Burkhart, C. A., Kavallaris, M., & Band, H. S. (2001). The role of beta-tubulin isotypes in resistance to antimitotic drugs. *Biochim Biophysica Acta*, *1471*, O1–O9. https://doi.org/10.1016/s0304-419x(00)00022-6

Cabral, F., Abraham, I., & Gottesman, M. M. (1982). Revertants of a Chinese hamster ovary cell mutant with an altered beta-tubulin: Evidence that the altered tubulin confers both colcemid resistance and temperature sensitivity on the cell. *Molecular Cell Biology*, *2*, 720–729. https://doi.org/10.1128/mcb.2.6.720

Da Silva, A. W. S., & Vranken, W. F. (2012). ACPYPE-Antechamber python parser interface. *BMC Research Notes*, *5*, 1–8. https://doi.org/10.1186/1756-0500-5-367

Dahlström, B., Mellstrand, T., Löfdahl, C. G., & Johansson, M. (1982). Pharmakokinetic properties of noscapine. *European Journal of Clinical Pharmacology*, *22*, 535–539. https://doi.org/10.1007/BF00609627

Darden, T., York, D., & Pedersen, L. (1993). Particle mesh ewald: An N· log (N) method for ewald sums in large systems. *Journal of Chemical Physics*, *98*, 10089–10092. https://doi.org/10.1063/1.464397

Dash, S. G., Suri, C., Nagireddy, P., Kantevari, S., & Naik, P. K. (2020). Rational design of 9-vinyl-phenyl noscapine as potent tubulin binding anticancer agent and evaluation of the effects of its combination on Docetaxel. *Journal of Biomolecular Structure and Dynamics*, 1–14.

Essmann, U., Perera, L., Berkowitz, M. L., Darden, T., Lee, H., & Pedersen, L. G. (1995). A smooth particle mesh ewald method. *Journal of Chemical Physics*, *103*, 8577–8593. https://doi.org/10.1063/1.470117

Friesner, R. A., Banks, J. L., Murphy, R. B., Halgren, T. A., Klicic, J. J., Mainz, D. T., Repasky, M. P., Knoll, E. H., Shelley, M., Perry, J. K., & Shaw, D. E. (2004). Glide: A new approach for rapid, accurate docking and scoring. 1. Method and assessment of docking accuracy. *Journal of Medicinal Chemistry*, *47*, 1739–1749. https://doi.org/10.1021/jm0306430

Halgren, T. A., Murphy, R. B., Friesner, R. A., Beard, H. S., Frye, L. L., Pollard, W. T., & Banks, J. L. (2004). Glide: A new approach for rapid, accurate docking and scoring. 2. Enrichment factors in database screening. *Journal of Medicinal Chemistry*, *47*, 1750–1759. https://doi.org/10.1021/jm030644s

Hamel, E., & Lin, C. M. (1981). Glutamate-induced polymerization of tubulin: Characteristics of the reaction and application to the large-scale purification of tubulin. *Archives of Biochemistry and Biophysics*, *209*, 29–40. https://doi.org/10.1016/0003-9861(81)90253-8

Hornak, V., Abel, R., Okur, A., Strockbine, B., Roitberg, A., & Simmerling, C. (2006). Comparison of multiple amber force fields and development of improved protein backbone parameters. *Proteins: Structure, Function, and Bioinformatics*, *65*, 712–725. https://doi.org/10.1002/prot.21123

Jackson, T., Chougule, M. B., Ichite, N., Patlolla, R. R., & Singh, M. (2008). Antitumor activity of noscapine in human non-small cell lung cancer xenograft model. *Cancer Chemotherapy Pharmacology*, *63*, 117–126. https://doi.org/10.1007/s00280-008-0720-z

Jain, N., Yada, D., Shaik, T. B., Vasantha, G., Reddy, P. S., Kalivendi, S. V., & Sreedhar, B. (2011). Synthesis and antitumor evaluation of nitrovinyl biphenyls: Anticancer agents based on allocolchicines. *ChemMedChem*, *6*, 859–868. https://doi.org/10.1002/cmdc.201100019

Jakalian, A., Bush, B. L., Jack, D. B., & Bayly, C. I. (2000). Fast, efficient generation of high-quality atomic charges. am1-bcc model: I. Method. *Journal of Computational Chemistry*, *21*, 132–146. https://doi.org/10.1002/(SICI)1096-987X(20000130)21:2<132:AID-JCC5>3.0.CO;2-P

Jakalian, A., Jack, D. B., & Bayly, C. I. (2002). Fast, efficient generation of high-quality atomic charges. am1-bcc model: Ii. parameterization and validation. *Journal of Computational Chemistry*, *23*, 1623–1641. https://doi.org/10.1002/jcc.10128

Jensen, L. N., Christrup, L. L., Jacobsen, L., Bonde, J., & Bundgaard, H. (1992). Relative bioavailability in man of noscapine administered in lozenges and mixture. *Acta Pharmaceutica Nordica*, *4*, 309–312.

Jordan, M. A., & Wilson, L. (2004). Microtubules as a target for anticancer drugs. *Nature Reviews Cancer*, *4*, 253–265. https://doi.org/10.1038/nrc1317

Karlsson, M. O., Dahlström, B., Eckernäs, S. Å., Johansson, M., & Alm, A. T. (1990). Pharmacokinetics of oral noscapine. *European Journal of Clinical Pharmacology*, *39*(3), 275–279. https://doi.org/10.1007/BF00315110

Karna, P., Rida, P. C., Pannu, V., Gupta, K. K., Dalton, W. B., Joshi, H., Yang, V. W., Zhou, J., & Aneja, R. (2011). A novel microtubulemodulating noscapinoid triggers apoptosis by inducing spindle multipolarity via centrosome amplification and declustering. *Cell Death & Differentiation*, *18*, 632–644. https://doi.org/10.1038/cdd.2010.133

Ke, Y., Ye, K., Grossniklaus, H. E., Archer, D. R., Joshi, H. C., & Kapp, J. A. (2000). Noscapine inhibits tumor growth with little toxicity to normal tissues or inhibition of immune responses. *Cancer*

Immunology Immunotherapy, *49*, 217–225. https://doi.org/10.1007/s002620000109

Kollman, P. A., Massova, I., Reyes, C., Kuhn, B., Huo, S., Chong, L., Lee, M., Lee, T., Duan, Y., Wang, W., & Donini, O. (2000). Calculating structures and free energies of complex molecules: Combining molecular mechanics and continuum models. *Accounts of Chemical Research*, *33*, 889–897. https://doi.org/10.1021/ar000033j

Landen, J. W., Hau, V., Wang, M., Davis, T., Ciliax, B., Wainer, B. H., Van Meir, E. G., Glass, J. D., Joshi, H. C., & Archer, D. R. (2004). Noscapine crosses the blood-brain barrier and inhibits glioblastoma growth. *Clinical Cancer Research*, *10*, 5187–5201. https://doi.org/10.1158/1078-0432.CCR-04-0360

Landen, J. W., Lang, R., McMahon, S. J., Rusan, N. M., Yvon, A. M., Adams, A. W., Sorcinelli, M. D., Campbell, R., Bonaccorsi, P., Ansel, J. C., & Archer, D. R. (2002). Noscapine alters microtubule dynamics in living cells and inhibits the progression of melanoma. *Cancer Research*, *62*, 4109–4114.

Liu, B., Staren, E. D., Iwamura, T., Appert, H. E., & Howard, J. M. (2001). Mechanisms of taxotere-related drug resistance in pancreatic carcinoma. *Journal of Surgical Research*, *99*, 179–186. https://doi.org/10.1006/jsre.2001.6126

Manchukonda, N. K., Naik, P. K., Santoshi, S., Lopus, M., Joseph, S., Sridhar, B., & Kantevari, S. (2013). Rational design, synthesis, and biological evaluation of third generation α-noscapine analogues as potent tubulin binding anti-cancer agents. *PLoS One*, *8*, e77970. https://doi.org/10.1371/journal.pone.0077970

Manchukonda, N. K., Naik, P. K., Sridhar, B., & Katevari, S. (2014). Synthesis and biological evaluation of novel biaryl type α-noscapine congeners. *Bioorganic Medicinal Chemistry Letter*, *24*, 5752–5757. https://doi.org/10.1016/j.bmcl.2014.10.046

Martindale, P. (1977). *The extra pharmacopeia*, A. Wade (ed), 27th ed. (p. 1250). The Pharmaceutical Press.

Meher, R. K., Nagireddy, P. K. R., Pragyandipta, P., Kantevari, S., Singh, S. K., Kumar, V., & Naik, P. K. (2021). In silico design of novel tubulin binding 9-arylimino derivatives of noscapine, their chemical synthesis and cellular activity as potent anticancer agents against breast cancer. *Journal of Biomolecular Structure and Dynamics*, *25*, 1–12. https://doi.org/10.1080/07391102.2021.1889668

Mishra, R. C., Karna, P., Gundala, S. R., Pannu, V., Stanton, R. A., Gupta, K. K., Robinson, M. H., Lopus, M., Wilson, L., Henary, M., & Aneja, R. (2011). Second generation benzofuranone ring substituted noscapine analogs: Synthesis and biological evaluation. *Biochemical Pharmacology*, *82*, 110–121. https://doi.org/10.1016/j.bcp.2011.03.029

Naik, P. K., Chatterji, B. P., Vangapandu, S. N., Aneja, R., Chandra, R., Kanteveri, S., & Joshi, H. C. (2011). Rational design, synthesis and biological evaluations of amino-noscapine: A high affinity tubulin-binding noscapinoid. *Journal of Computer Aided Molecular Design*, *25*, 443–454. https://doi.org/10.1007/s10822-011-9430-4

Naik, P. K., Lopus, M., Aneja, R., Vangapandu, S. N., & Joshi, H. C. (2012). In silico inspired design and synthesis of a novel tubulin-binding anti-cancer drug: Folate conjugated noscapine (Targetin). *Journal of Computer Aided Molecular Design*, *26*, 233–247. https://doi.org/10.1007/s10822-011-9508-z

Naik, P. K., Santoshi, S., Rai, A., & Joshi, H. C. (2011). Molecular modelling and competition binding study of Br-noscapine and colchicine provide insight into noscapinoid–tubulin binding site. *Journal of Molecular Graphics and Modelling*, *29*, 947–955. https://doi.org/10.1016/j.jmgm.2011.03.004

Oliva, M. A., Prota, A. E., Rodríguez-Salarichs, J., Bennani, Y. L., Jiménez-Barbero, J., Bargsten, K., Canales, Á., Steinmetz, M. O., & Díaz, J. F. (2020). Structural basis of noscapine activation for tubulin binding. *Journal of Medicinal Chemistry*, *63*, 8495–8501. https://doi.org/10.1021/acs.jmedchem.0c00855

Panda, D., Chakrabarti, G., Hudson, J., Pigg, K., Miller, H. P., Wilson, L., & Himes, R. H. (2000). Suppression of microtubule dynamic instability and treadmilling by deuterium oxide. *Journal of Biochemistry*, *39*, 5075–5081. https://doi.org/10.1021/bi992217f

Santoshi, S., Manchukonda, N. K., Suri, C., Sharma, M., Sridhar, B., Joseph, S., Lopus, M., Kantevari, S., Baitharu, I., & Naik, P. K. (2015). Rational design of biaryl pharmacophore inserted noscapine derivatives as potent tubulin binding anticancer agents. *Journal of Computer Aided Molecular Design*, *29*, 249–270. https://doi.org/10.1007/s10822-014-9820-5

Santoshi, S., & Naik, P. K. (2014). Molecular insight of isotypes specific β-tubulin interaction of tubulin heterodimer with noscapinoids. *Journal of Computer Aided Molecular Design*, *28*, 751–763. https://doi.org/10.1007/s10822-014-9756-9

Santoshi, S., Naik, P. K., & Joshi, H. C. (2011). Rational design of novel anti-microtubule agent (9-azido-noscapine) from quantitative structure activity relationship (QSAR) evaluation of noscapinoids. *Journal of Biomolecular Screening*, *16*, 1047–1058. https://doi.org/10.1177/1087057111418654

Sung, B., Ahn, K. S., & Aggarwal, B. B. (2010). Noscapine, a benzylisoquinoline alkaloid, sensitizes leukemic cells to chemotherapeutic agents and cytokines by modulating the NF-kappaB signaling pathway. *Cancer Research*, *70*, 3259–3268. https://doi.org/10.1158/0008-5472.CAN-09-4230

Wang, J., Wolf, R. M., Caldwell, J. W., Kollman, P. A., & Case, D. A. (2004). Development and testing of a general amber force field. *Journal of Computational Chemistry*, *25*, 1157–1174. https://doi.org/10.1002/jcc.20035

Ye, K., Ke, Y., Keshava, N., Shanks, J., Kapp, J. A., Tekmal, R. R., Petros, J., & Joshi, H. C. (1998). Opium alkaloid noscapine is an antitumor agent that arrests metaphase and induces apoptosis in dividing cells. *Proceedings of the National Academy of Sciences*, *95*, 1601–1606. https://doi.org/10.1073/pnas.95.4.1601

Zhou, J., Gupta, K., Aggarwal, S., Aneja, R., Chandra, R., Panda, D., & Joshi, H. C. (2003). Brominated derivatives of noscapine are potent microtubule-interfering agents that perturb mitosis and inhibit cell proliferation. *Molecular Pharmacology*, *63*, 799–807. https://doi.org/10.1124/mol.63.4.799

Zhou, J., Gupta, K., Yao, J., Ye, K., Panda, D., Giannakakou, P., & Joshi, H. C. (2002). Paclitaxel-resistant human ovarian cancer cells undergo c-Jun NH2-terminal kinase-mediated apoptosis in response to noscapine. *Journal of Biological Chemistry*, *277*, 39777–39785. https://doi.org/10.1074/jbc.M203927200

Zhou, J., Panda, D., Landen, J. W., Wilson, L., & Joshi, H. C. (2002). Minor alteration of microtubule dynamics causes loss of tension across kinetochore pairs and activates the spindle checkpoint. *Journal of Biological Chemistry*, *277*, 17200–17208. https://doi.org/10.1074/jbc.M110369200

Zhou, R., Friesner, R. A., Ghosh, A., Rizzo, R. C., Jorgensen, W. L., & Levy, R. M. (2001). New linear interaction method for binding affinity calculations using a continuum solvent model. *The Journal of Physical Chemistry B*, *105*, 10388–10397. https://doi.org/10.1021/jp011480z

Zhou, J., Liu, M., Luthra, R., Jones, J., Aneja, R., Chandra, R., Tekmal, R. R., & Joshi, H. C. (2005). EM012, a microtubule-interfering

agent, inhibits the progression of multidrug-resistant human ovarian cancer both in cultured cells and in athymic nude mice. *Cancer Chemotherapy and Pharmacology*, *55*, 461–465.

SUPPORTING INFORMATION

Additional supporting information may be found online in the Supporting Information section.

How to cite this article: Meher, R. K., Pragyandipta, P., Pedapati, R. K., Nagireddy, P. K. R., Kantevari, S., Nayek, A. K., & Naik, P. K. (2021). Rational design of novel *N*-alkyl amine analogues of noscapine, their chemical synthesis and cellular activity as potent anticancer agents. *Chemical Biology & Drug Design*, 00, 1–21. https://doi.org/10.1111/cbdd.13901